Watershed modeling in the Tyrrhena Terra region of Mars

Scott C. Mest,[1,2] David A. Crown,[1] and William Harbert[3]

Received 9 May 2009; revised 13 December 2009; accepted 29 January 2010; published 1 September 2010.

[1] Watershed analyses from high-resolution image (Viking, Mars Orbiter Camera, and Thermal Emission Imaging System) and topographic (Mars Orbiter Laser Altimeter [MOLA]) data are used to qualitatively and quantitatively characterize highland fluvial systems and analyze the role of water in the evolution of Tyrrhena Terra (13°S–30°S, 265°W–280°W), Mars. In this study, Geographical Information System software is used in conjunction with MOLA Digital Elevation Models to delineate drainage basin divides, extract valley networks, and derive basin and network morphometric parameters (e.g., drainage density, stream order, bifurcation ratio, and relief morphometry) useful in characterizing the geologic and climatic conditions of watershed formation, as well as for evaluating basin "maturity" and processes of watershed development. Model-predicted valley networks and watershed boundaries, which are dependent on the degree to which pixel sinks are filled in the topographic data set and a channelization threshold, are evaluated against image and topographic data, slope maps, and detailed maps of valley segments from photogeologic analyses. Valley morphologies, crater/valley relationships, and impact crater distributions show that valleys in Tyrrhena Terra are ancient. Based on geologic properties of the incised materials, valley and network morphologies, morphometric parameters, and the presence of many gullies heading at or near-crater rim crests, surface runoff, derived from rainfall or snowmelt, was the dominant erosional process; sapping may have only played a secondary role in valley formation in Tyrrhena Terra. Furthermore, spatial and temporal relationships of dissected highland materials and impact craters, suggests widespread, but relatively short-lived, erosion by runoff with most activity in the Noachian period.

Citation: Mest, S. C., D. A. Crown, and W. Harbert (2010), Watershed modeling in the Tyrrhena Terra region of Mars, *J. Geophys. Res.*, *115*, E09001, doi:10.1029/2009JE003429.

1. Introduction

[2] Since the Mariner 9 and Viking 1 and 2 missions [e.g., *McCauley et al.*, 1972; *Masursky*, 1973; *Milton*, 1973], intricate systems of valleys dissecting the ancient cratered highlands have become some of the most intriguing features on Mars, suggesting water may have played a major role in modifying the highlands. Although liquid water is not stable at the surface of Mars under current conditions, the presence of fluvial valleys indicates liquid water was likely present at some earlier time. Most valley networks (~99%) are found in the highlands and may be as old as the materials they dissect [*Pieri*, 1976, 1980; *Carr and Clow*, 1981; *Mars Channel Working Group*, 1983; *Baker and Partridge*, 1986; *Grant and Schultz*, 1990; *Craddock and Maxwell*, 1993; *Maxwell and Craddock*, 1995; *Carr and Chuang*, 1997; *Grant*, 2000]. Although many hypotheses have been proposed regarding the origins of Martian valley networks, their formation is not yet well understood.

[3] Terrestrial drainage networks typically form in response to combinations of precipitation-driven erosion and groundwater sapping [*Ritter et al.*, 1995]. Similar processes have been proposed to explain the origin of Martian valley networks [e.g., *Pieri*, 1976, 1980; *Carr and Clow*, 1981; *Gulick and Baker*, 1990; *Craddock and Maxwell*, 1993; *Grant and Schultz*, 1993, 1994; *Maxwell and Craddock*, 1995; *Carr*, 1995, 1996; *Grant*, 2000; *Craddock and Howard*, 2002; *Grant and Parker*, 2002]; however, the relative contributions of runoff and sapping to valley network formation are not known. This is an especially important issue for understanding Mars' evolution, given ongoing debates about climate change and whether the fluvial history of the surface is dominated by atmospheric or subsurface cycling of volatiles.

[4] Geologic mapping and geomorphic analyses in Tyrrhena Terra along the north rim of Hellas basin (13°S–30°S, 265°W–280°W) (Figure 1) have revealed a complex history of impact cratering and modification by fluvial and eolian activity [*Schaber*, 1977; *Greeley and Guest*, 1987; *Tanaka and Leonard*, 1995; *Mest*, 2004; *Mest and Crown*, 2006]. High-resolution Mars Orbiter Camera (MOC), Thermal

[1]Planetary Science Institute, Tucson, Arizona, USA.
[2]Planetary Geodynamics Laboratory, NASA Goddard Space Flight Center, Greenbelt, Maryland, USA.
[3]Department of Geology and Planetary Science, University of Pittsburgh, Pittsburgh, Pennsylvania, USA.

0148-0227/10/2009JE003429

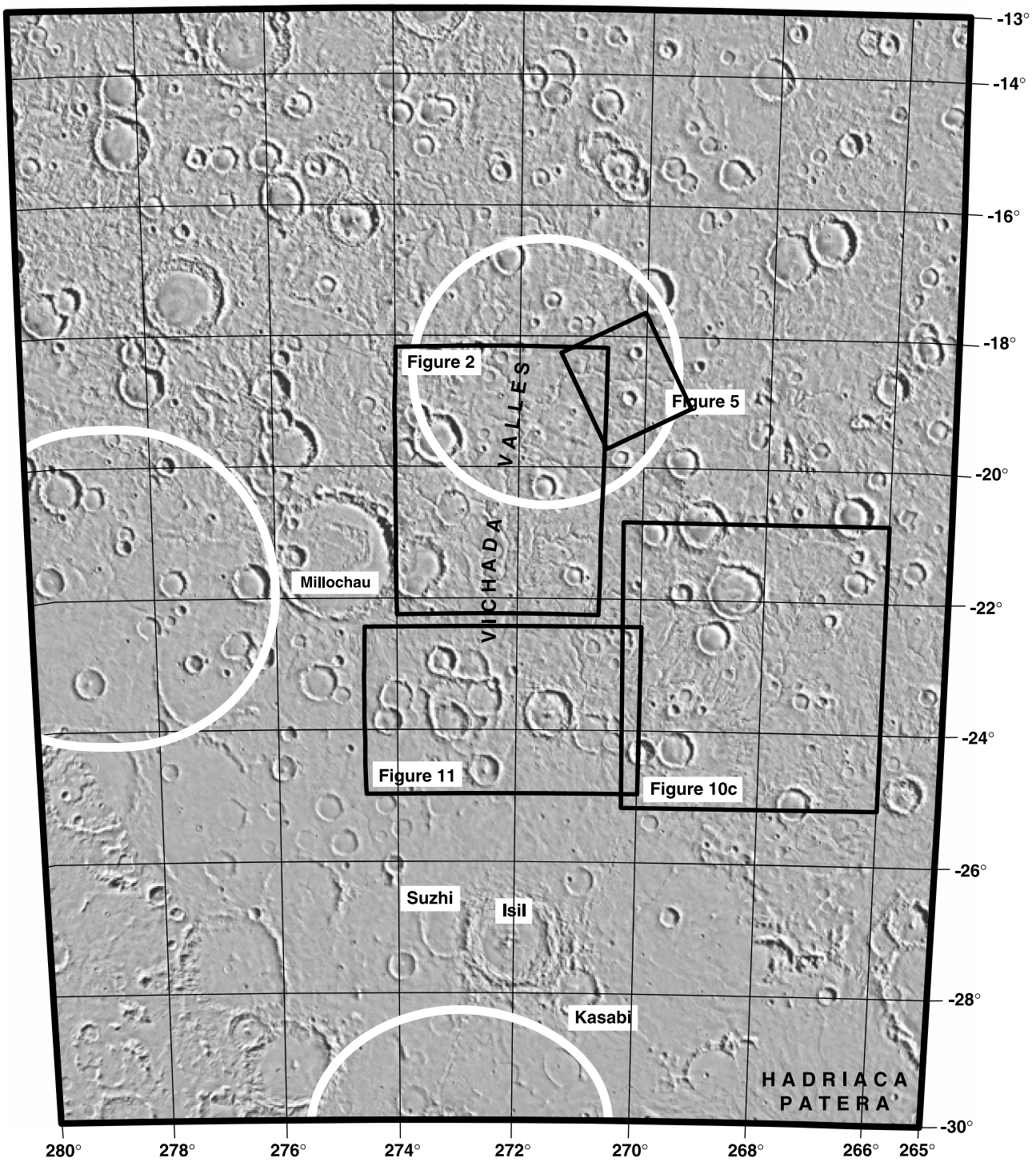

Figure 1. Viking MDIM 2.0 photomosaic showing the highlands of Tyrrhena Terra, north of Hellas impact basin. The locations of three possible impact basins identified using MOLA [*Frey et al.*, 2000] are shown (white circles). The locations of Figures 2, 5, 10c, and 11 are shown. North is to the top in this and all subsequent figures unless noted otherwise; projection is Mercator.

Emission Imaging System (THEMIS), and Viking Orbiter images and Mars Orbiter Laser Altimeter (MOLA) topographic data have been used to characterize highland fluvial systems and analyze the role of water in the evolution of the highlands of Tyrrhena Terra. Fluvial features in this region include widespread, well-integrated valley networks, such as Vichada Valles, smaller networks and single channels, and gullies incised along the rims of impact craters [*Mest and Crown*, 2005, 2006]. Geographical Information System (GIS) software has been used in conjunction with MOLA Digital Elevation Models (DEMs) to delineate drainage basin divides, extract valley networks, and derive

basin and network morphometric parameters useful in characterizing basin "maturity" and processes of watershed development [*Mest et al.*, 2001a, 2001b, 2002]. This paper describes the methodology used and presents the results obtained for watersheds in Tyrrhena Terra. The model-predicted networks and the parameters calculated from these data are compared to data derived from fluvial systems mapped by *Mest* [2004] and *Mest and Crown* [2006]. The abundance and widespread nature of fluvial features within Tyrrhena Terra have significant implications for past Martian environmental conditions, and characterization of these fluvial features by mapping and hydrologic modeling is necessary to fully understand the nature of Martian fluvial activity and the history of Mars' climate.

2. Background

[5] Martian valley networks consist of channels with few tributaries to complex, well-developed stream patterns, and are interpreted to have formed by flowing water [e.g., *Milton*, 1973; *Pieri*, 1976, 1980; *Mars Channel Working Group*, 1983; *Carr*, 1996; *Malin and Carr*, 1999; *Craddock and Howard*, 2002]. Many previous studies have suggested that Mars' climate has remained relatively unchanged (i.e., cold and dry), with most valley networks formed predominantly by groundwater sapping or seepage-fed runoff [*Pieri*, 1976, 1980; *Carr and Clow*, 1981; *Mars Channel Working Group*, 1983; *Baker and Partridge*, 1986 (pristine valleys); *Kochel and Piper*, 1986; *Carr*, 1995, 1996; *Carr and Chuang*, 1997; *Malin and Edgett*, 2000; *Cabrol and Grin*, 2001; *Stepinski and Collier*, 2004a, 2004b; *Stepinski and Coradetti*, 2004]. To accommodate for Mars' low atmospheric pressure, some models invoke geothermal heating to drive sapping processes [*Brakenridge et al.*, 1985; *Clifford*, 1993; *Gulick*, 1998, 2001; *Tanaka et al.*, 1998; *Malin and Carr*, 1999; *Carr and Malin*, 2000; *Goldspiel and Squyres*, 2000]. Morphologically, some Martian highland networks display reticulate patterns, suggesting structural control, and form open, branching systems with few tributaries; these characteristics are indicative of sapping dominated systems [*Pieri*, 1976, 1980; *Carr*, 1995, 1996]. Also, Martian valleys with steep-walled, U-shaped cross sections and stubby tributaries with theater-headed terminations are morphologically similar to sapping valleys on the Colorado Plateau [*Pieri*, 1976, 1980; *Carr and Clow*, 1981; *Mars Channel Working Group*, 1983; *Carr*, 1995, 1996; *Malin and Carr*, 1999]. However, topographic profiles across highland valleys [*Goldspiel et al.*, 1993] were shown to have "smoothly curved" cross sections and lack the steep walls typical of terrestrial sapping valleys; morphologically, these highland valleys more closely resemble valleys formed or modified by surface runoff. *Goldspiel et al.* [1993] suggested that cross sections of valleys formed by sapping and runoff processes on Mars could be similar due to valley formation in highly fractured megaregolith or unconsolidated ash versus competent rock and the extensive duration of valley modification.

[6] *Craddock and Howard* [2002] noted that many studies advocating sapping-dominated valley formation do not account for valleys that head at, or near, the tops of massifs or the rims of impact craters. Many highland impact craters preserve a record of extensive erosion by displaying dissected ejecta deposits, smooth floors, and (or) interior and exterior valleys along their rims [*Craddock and Maxwell*, 1993]. Both sapping and precipitation may have eroded these impact craters and the surrounding highlands. Precipitation would have eroded ejecta by sheetwash; channels along the exterior and interior rims of the craters could have formed by combinations of runoff and sapping, provided aquifers were recharged by precipitation, and an adequate hydrostatic head was available [*Craddock and Maxwell*, 1993; *Craddock et al.*, 1997a, 1997b, 1999]. *Grant* [2000] and *Grant and Parker* [2002] have shown that valley networks in the Margaritifer Sinus region of Mars have lower drainage densities than terrestrial basins formed by runoff. However, groundwater sapping cannot be inferred either, as these densities do not reflect resurfacing of some valleys and the resolutions at which the measurements were taken are not comparable to terrestrial mapping resolutions. Some studies have considered a hybrid process whereby precipitation dominates valley formation via surface runoff and recharges subsurface aquifers, which contribute to network formation by sapping [*Baker and Partridge*, 1986 (degraded valleys); *Craddock and Maxwell*, 1993; *Craddock et al.*, 1997a, 1997b, 1999; *Grant*, 2000; *Hynek and Phillips*, 2001; *Mest and Crown*, 2001a, 2006; *Craddock and Howard*, 2002; *Grant and Parker*, 2002; *Irwin and Howard*, 2002; *Stepinski et al.*, 2002a, 2002b; *Irwin et al.*, 2004]. Other studies have suggested that snowmelt, resulting from a warmer climate or geothermal heating, could have formed many valleys in the highlands and on the flanks of volcanoes [*Gulick et al.*, 1997; *Stepinski et al.*, 2002a, 2002b; *Carr and Head*, 2004; *Fassett and Head*, 2007].

3. Geologic Setting

[7] Tyrrhena Terra displays a shallow (0.23°) southward-trending slope toward Hellas basin. It is likely that the impact event forming Hellas basin established this regional slope as well as structural patterns that have influenced the geologic history of this region, with potential contributions from three buried and degraded impact basins identified by *Frey et al.* [2000] (Figure 1). These basins would have acted as sinks in which water and alluvial and eolian sediments could have accumulated. Hellas basin exhibits more than 10 km of relief [*Smith et al.*, 1999] with a maximum elevation of ~3 km along the north and west rims and a minimum elevation of ~–8 km on its western floor. From mapping, geologic units in Tyrrhena Terra are believed to consist of a suite of interlayered sedimentary, volcanic, and impact-related materials [*Schaber*, 1977; *Greeley and Guest*, 1987; *Mest and Crown*, 2006] that are believed to be laterally and vertically variable [*Mest and Crown*, 2001a] both regionally and within individual drainage basins, thus, affecting the permeability and erodibility of these materials.

[8] This area contains a high density of impact craters that range in diameter from the limits of MOC resolution to over 100 km and display variations in preservation state (Figure 1). Most craters are moderately to highly degraded, and even many "fresh" craters have experienced some degree of modification. Many of the larger craters in Tyrrhena Terra, regardless of their preservation state, contain deposits that cover their floors. These deposits, determined by crater size-frequency distribution statistics and crosscutting and

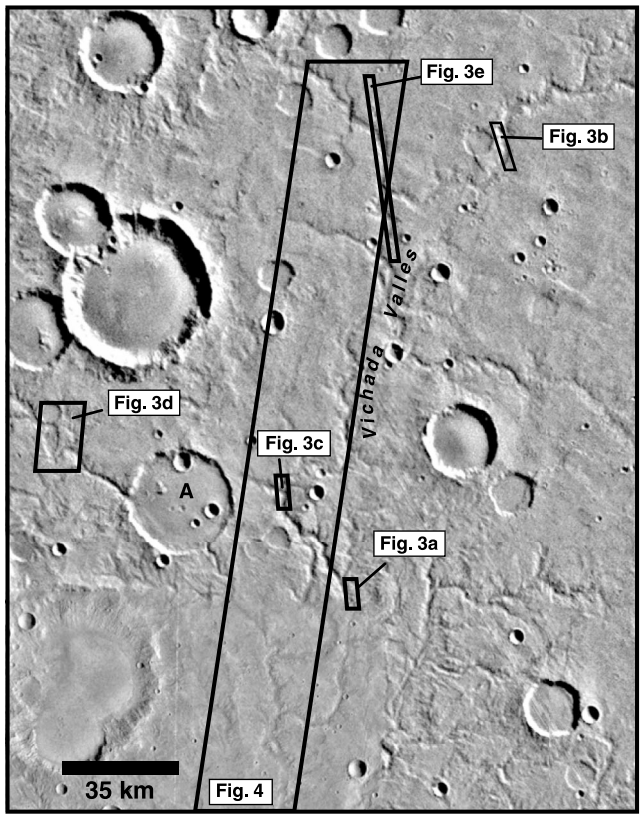

Figure 2. Part of Viking Mars Transverse Mercator quadrangle -20272 showing intercrater plains in Tyrrhena Terra. Here the plains are dissected by large-scale, well-incised systems of valleys, including Vichada Valles, and exhibit many impact craters preserved to various degrees. Crater "A" (20.7°S, 273.1°W; D = 34 km) is breached by valleys along its western (inlet?) and southeast (outlet?) rims. MOLA data show that the western breach is ~200 m wider and 50 m deeper than the southeast breach (widths = 1100 m and 900 m and depths = 100 m and 50 m, respectively), and the floor of the southeast breach is ~100 m higher in elevation than the floor of the western breach. Most craters in the area contain smooth (at Viking Orbiter resolutions) deposits presumably consisting of materials eroded from the crater rim and deposited via fluvial (as in the case of crater A) and (or) eolian processes. The locations of Figures 3 and 4 are shown. Figure centered at 20.0°S, 272.2°W; illumination from upper right.

superposition relationships to be Late Noachian to Early Hesperian in age [*Mest and Crown*, 2006], have several likely origins, such as (1) eroded crater rim and wall materials deposited via gullies and (or) by mass wasting, and in some cases forming alluvial fans [e.g., *Moore and Howard*, 2005], and (or) (2) highland materials deposited via valleys that breached crater rims. Many crater interiors, such as Millochau [*Mest and Crown*, 2005] and several unnamed craters in Tyrrhena Terra [*Mest and Crown*, 2006], may also contain deposits emplaced within playas or long-standing lake systems. Potential paleo-lacustrine environments within craters have been identified on Mars in numerous studies [e.g., *Cabrol and Grin*, 2001; *Forsythe and Blackwelder*, 1998; *Fassett and Head*, 2008], and several recent studies [e.g., *Mest and Crown*, 2001b; *Moore and Wilhelms*, 2001; *Ansan and Mangold*, 2004; *Crown et al.*, 2005, 2009; *Wilson et al.*, 2007; *Mest et al.*, 2008] have suggested lacustrine deposits might be found within many of the craters surrounding Hellas basin. In addition, recent data from the Observatoire pour la Minéralogie, l'Eau, les Glaces et l'Activité (OMEGA) and Compact Reconnaissance Imaging Spectrometer for Mars (CRISM) instruments show several sites in Tyrrhena Terra where phyllosilicates have been detected [*Bibring et al.*, 2006; *Costard et al.*, 2006; *Pelkey et al.*, 2007], which provide evidence that water existed long enough to produce hydrated minerals.

[9] Tyrrhena Terra shows abundant evidence for erosion and deposition by fluvial and eolian processes. This highland region contains dendritic to (sub)parallel valley networks that dissect an extensive Noachian-aged intercrater plains unit [*Mest and Crown*, 2006]. Vichada Valles, which is composed of at least twelve subbasins, is the most extensive network in the area and the major watershed for this part of the highlands [*Craddock and Maxwell*, 1993; *Carr and Chuang*, 1997; *Cabrol and Grin*, 2001; *Mest et al.*, 2002; *Mest*, 2004; *Mest and Crown*, 2006]; several smaller networks and individual channels are also found. Much of the erosion that formed valleys and eroded craters in this area is believed to have occurred in the Late Noachian Epoch and continued into the Early Hesperian Epoch [*Greeley and Guest*, 1987; *Tanaka and Leonard*, 1995; *Leonard and Tanaka*, 2001; *Mest and Crown*, 2006]. Previous researchers [e.g., *Carr*, 1995, 1996] have suggested some valleys in Tyrrhena Terra formed by combinations of runoff-induced mass wasting and sapping processes; however, questions regarding the ability of sapping to be sustained along crater rims are applicable here. Furthermore, the ability to sustain an interconnected aquifer system in Tyrrhena Terra is problematic where interlayered sequences of volcanic, sedimentary, and impact materials [*Mest and Crown*, 2006] would likely restrict groundwater flow. The most recent activity in the area is eolian mobilization and deposition of sediments in low-lying areas.

3.1. Geomorphology of Tyrrhena Terra Valley Networks

[10] From image analyses, valley networks in Tyrrhena Terra display dendritic to (sub)parallel patterns and dissect large portions of these highlands. At some point in the past, Vichada Valles (Figure 2) presumably extended into Hellas basin, but evidence of this extension is obscured by a group of large craters at 24°S (Figure 1). Several smaller networks are incised in the surrounding highland terrain, some of which are separated from Vichada Valles by impact craters or ejecta. In this study, isolated networks have been treated as separate subbasins, but many were likely connected to Vichada Valles at one time. Most tributaries of Vichada Valles head within an elevation range of ~1.5–2.5 km. MOC images show that valleys display highly degraded morphologies with rounded banks, layers, or terraces along valley walls, and dune-forming sediments covering their floors (Figure 3) [*Mest and Crown*, 2006]. MOLA profiles show that most trunk valleys have fairly flat or gently sloping floors, and many tributaries are V-shaped in cross section; valley depths and widths range between ~70 to 200 m and ~0.9 to 10.5 km, respectively.

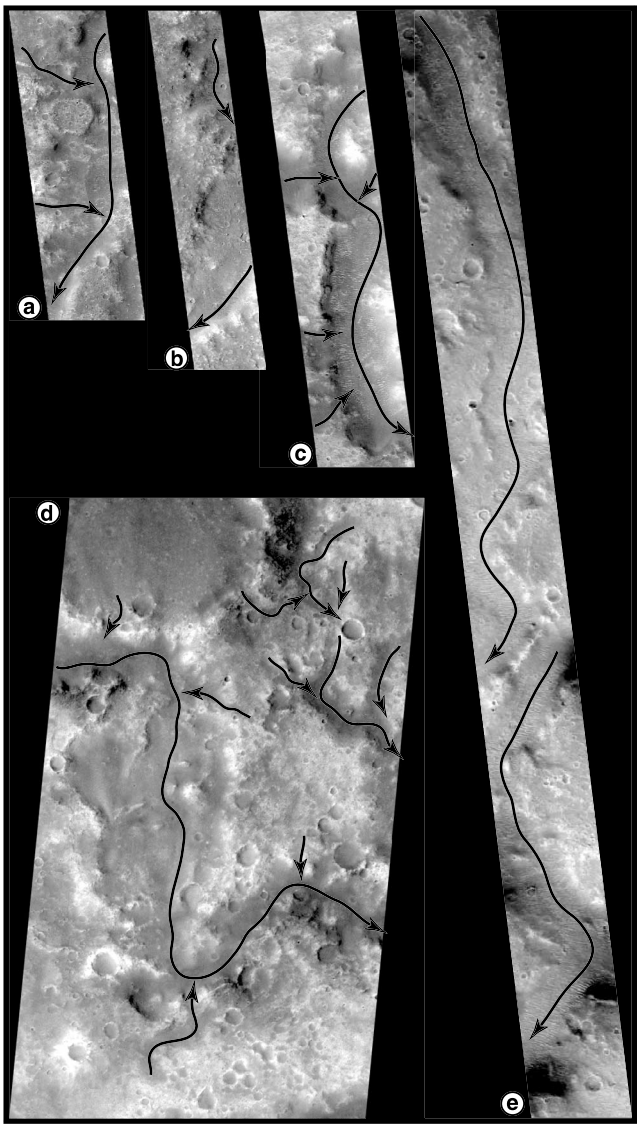

Figure 3. MOC narrow-angle images showing parts of the Vichada Valles system, including sections of the main channel (Figures 3a, 3c and 3e) and tributaries (Figures 3b, 3d and 3e), incised within intercrater plains material. All sections of valleys shown are filled to some degree with sediment; parallel sets of dunes oriented orthogonal to valley walls are visible in a, b, c, and e, suggesting this material has been mobile. Black arrows point in downstream direction. Images include (image number; image center; image width; resolution): (a) M03-03481; 21.0°S, 272.2°W; 2.88 km; 2.81 m/pixel. (b) M04-02305; 18.7°S, 271.5°W; 2.16 km; 2.82 m/pixel. (c) M08-02977; 20.7°S, 272.8°W; 2.88 km; 2.81 m/pixel. (d) AB1-09306; 20.4°S, 273.9°W; 10.79 km; 5.27 m/pixel. (e) E12-00204; 19.0°S, 272.0°W; 3.04 km; 5.94 m/pixel.

[11] The trunk valley of Vichada Valles branches and rejoins downstream several times along its course (Figure 4). *Carr* [1995, 1996] attributed this phenomenon to headward erosion of a sapping-type valley, in which random headward extension led to intersection of the valleys upstream. However, terracing, branching, and rejoining of larger valleys, and downstream variations in width and depth suggest that valley formation is more complex than can be explained by sapping alone and require a process involving higher, and generally fluctuating, discharges to cause lateral erosion of valley walls or meandering. In general, these features are not characteristic of sapping-dominated systems in which discharges are constant and valley width and depth remain relatively constant from head to mouth [*Carr*, 1995, 1996; *Goldspiel et al.*, 1993; *Goldspiel and Squyres*, 2000]. *Carr*

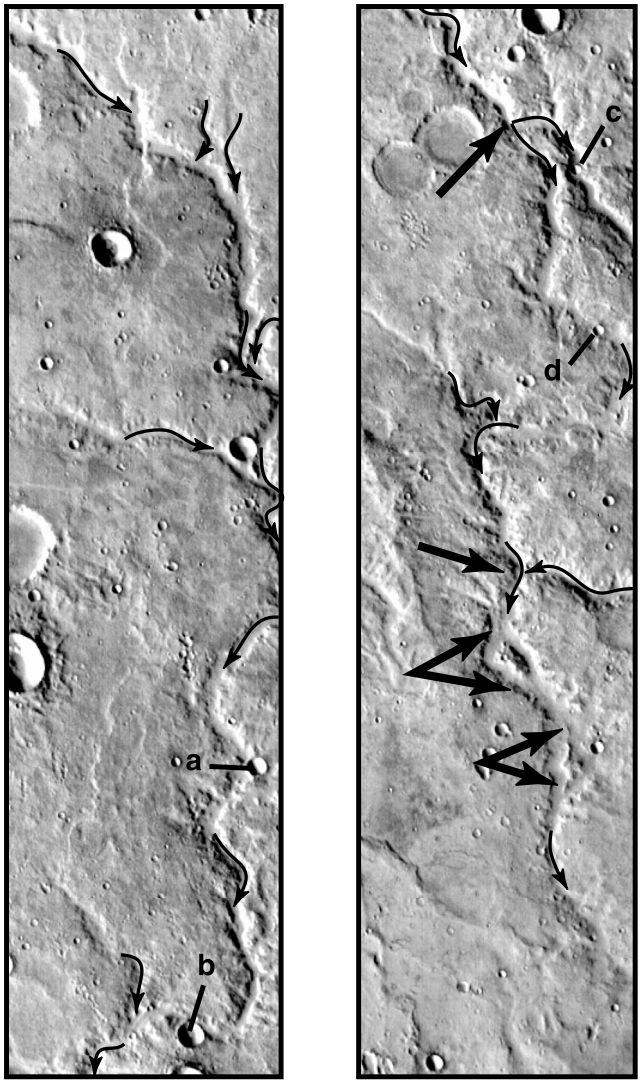

Figure 4. Part of THEMIS daytime IR image I07550002, split into (left) upper and (right) lower sections, showing the main valley of Vichada Valles. The lower section shows three locations where Vichada Valles branches and rejoins downstream (heavy black arrows). There are no obvious obstructions, such as an impact crater, along the valley that would cause diversion or redirection of flow to form these branches. In addition, (a–d) several craters are located either fully or partially within the main valley, but there is no evidence for ponding upstream or diversion of water around these obstructions, suggesting flow within the system was low or had ceased prior to formation of these craters. Thin black arrows point in the downstream direction.

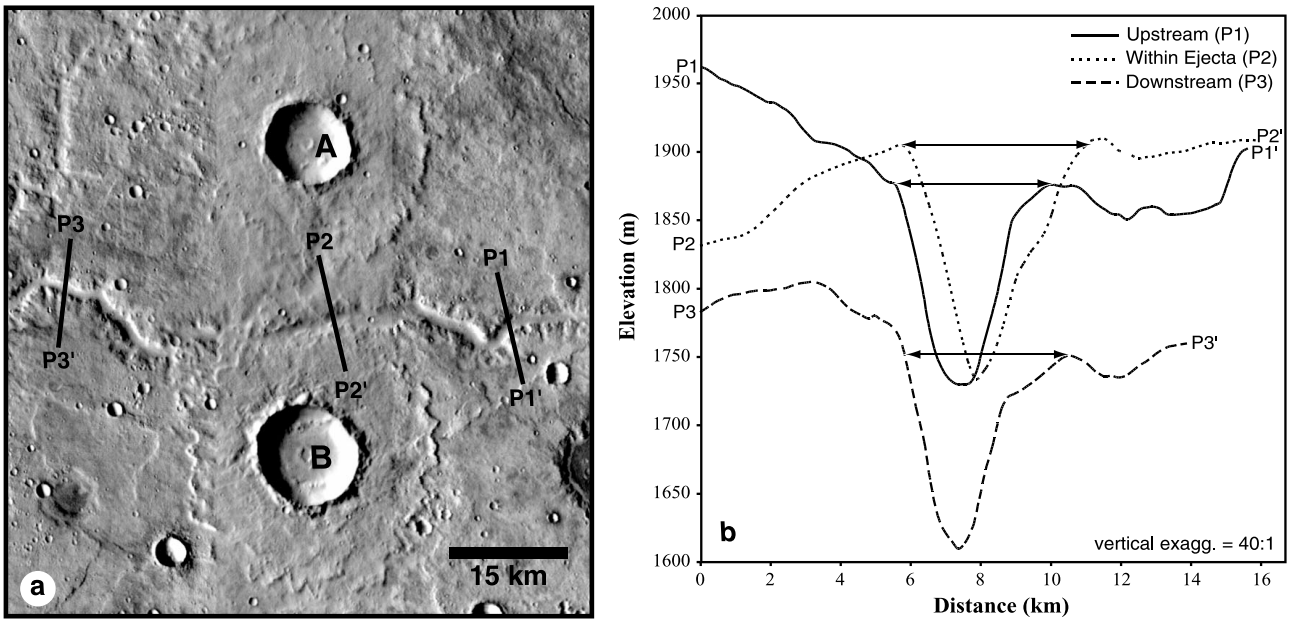

Figure 5. Part of Viking Orbiter image 625A25 showing a tributary of Vichada Valles in the plains between two large craters (A and B). The craters show ejecta blankets that either mantle a preexisting valley or are eroded by a valley; from available images, it is not clear whether ejecta material is present on the valley floor. Topographic profiles across this valley, from MOLA DEM (64 pix/deg), show the valley is ~25 m deeper and its floor is ~5 m higher in elevation where the valley crosses the ejecta (P2-P2′) compared to upstream (P1-P1′) and downstream (P3-P3′) from the ejecta [*Mest and Crown*, 2006]. Arrows indicate the top of the valley wall. There is no evidence for ponding or diversion of water, suggesting fluvial processes were active and ended prior to crater formation or that fluids moved easily through the valley following ejecta emplacement. North is to the upper right corner; image is centered at 18.5°S, 270.0°W; resolution = 239.82 m/pixel; illumination from right.

and Malin [2000] suggested that a section of one of Vichada Valles' tributaries (Figure 3d) resembles thermokarst terrain where alases (irregularly shaped, flat-floored, steep-sided hollows) grow and merge due to combined processes of surface drainage and melting ground ice. Although Viking images show a well-integrated system, they observed that MOC image AB1-09306 (Figure 3d) can be interpreted to show that subsequent processes "dominate" the appearance of Vichada Valles. Our analysis of Vichada Valles (Figures 2, 3, 4 and 5) indicates that the morphology observed in MOC image AB1-09306 is not typical of the system as a whole. This potential "thermokarst" morphology is not observed either upstream or downstream of the reach shown in AB1-09306, elsewhere within the Vichada Valles system, or in the highlands proximal to Vichada Valles. This reach of Vichada Valles may not have formed or been modified by thermokarst processes; rather, it appears to consist of a cluster of small impact craters that were breached, significantly eroded, and subsequently infilled with alluvial and eolian sediments. We attribute the overall morphology of Vichada Valles and its tributaries to a combination of fluvial erosion and minor mass wasting, overprinted by eolian infilling. Infilling is observed throughout the Vichada Valles system and may explain some regions that appear poorly integrated.

[12] Some valleys, particularly those that have no tributaries or form dense (sub)parallel networks, are smaller and appear less incised than Vichada Valles and other large dendritic systems in the region. The tributaries of these smaller systems typically head at crater rim crests and are generally not more than a few kilometers long. Their occurrence on relatively steep slopes results in more closely spaced first-order tributaries. For example, smaller networks in the eastern part of the study area empty into a buried crater basin (centered at 24.4°S, 269.0°W; Figure 1) that has subsequently accumulated large impact craters on its floor. None of these smaller networks are observed to intersect the trunk valley of Vichada Valles. Because many of these dense networks of valleys head at crater rim crests, *Carr* [1995, 1996] attributed their formation to sapping combined with minor components of surface runoff and mass wasting of water-saturated materials. The morphologic differences between these smaller networks and Vichada Valles could also be due to differences in age, lithology, and (or) slope.

3.2. Crosscutting Relationships Between Valleys and Impact Craters

[13] Impact craters dominate the local topography in Tyrrhena Terra. The impact structure, the fractured, brecciated, and recrystallized target materials and the impact ejecta may have had significant effects on any surface or subsurface flow of water. If clear temporal relationships between craters and fluvial valleys can be assessed from photogeologic analyses, it is possible to evaluate the topographic effects of craters that postdate fluvial activity and reconstruct the preimpact topography. Coverage of Tyrrhena

Terra by mostly low-resolution Viking Orbiter and few high-resolution MOC images makes identification of clear crosscutting relations between fluvial valleys and impact craters difficult. However, THEMIS images (Figure 4) allow relationships to be better characterized and help to evaluate spatial and temporal relationships between fluvial activity and cratering.

[14] Impact craters that superpose valleys do so typically by truncation or bisection by the impact structure or ejecta blanket. In most instances, craters and associated ejecta that intersect valleys show little evidence for modification by flow and indicate that valley formation largely preceded formation of most craters in the region. In some locations, however, valleys originate within ejecta materials, and some valleys appear to incise ejecta, though the origin of local relief within these valleys remains uncertain (Figure 5) [*Mest and Crown*, 2006].

[15] Impact craters exhibiting breached rims, such as crater "A" (Figure 2) are also observed but are rare. Crater "A" displays a relatively flat interior, an inlet valley breaching the western rim, and an outlet valley breaching the southeast rim [*Mest and Crown*, 2006], suggesting this crater may have provided temporary storage of water prior to exiting via the outlet breach. However, crater "A" shows no clear evidence, such as shorelines or benches, to indicate water level. Therefore, it is also possible that the "outlet" valley grew headward within the plains until it breached the crater rim.

[16] The relationships mentioned above suggest that some fluvial activity in the study area occurred prior to the end of Heavy Bombardment when most large impact craters formed. The eroded rims and ejecta blankets of many craters provide evidence for some later fluvial erosion. Crater size-frequency distributions for valley floor material [*Mest and Crown*, 2006] indicate that most fluvial activity ceased in the Late Noachian Epoch to Early Hesperian Epoch, suggesting that most valley formation in this part of the highlands is relatively old. This is similar to the results of *Maxwell and Craddock* [1995], in which the age of valley formation in the highlands of Mare Tyrrhenum (15°–30°, 260°W–270°W) was found to be Late Noachian to Early Hesperian.

[17] In terms of hydrologic modeling, determining the relationships described above is necessary to accurately interpret model results. If most impact craters formed prior to fluvial activity and valley incision, then the craters would create local topography that would control subsequent surface flow. If most impact craters formed after valley incision, then model-predicted valleys would follow the topography created by the older craters and should correlate with observed valleys only in areas where the effect of younger impact-generated topography was minimal. If cratering and valley incision were largely contemporaneous or significant numbers of craters both predated and postdated fluvial activity, then fluvial systems would be more difficult to reconstruct [*Irwin and Craddock*, 2001; *Irwin and Howard*, 2002; *Irwin and Maxwell*, 2003; *Irwin et al.*, 2002a, 2002b].

4. Methodology

[18] Hydrologic mapping has been combined with algorithmic extraction of valley networks to assess the hydrologic history of the Tyrrhena Terra region of Mars. This section first provides a general description of the image and topographic data sets used in this study, compilation of valley network maps for the region, and their manipulation within the Arc/Info-based Geographical Information System. The hydrologic modeling techniques, specifically Arc/Info GRID functions, are then described in detail. In order to evaluate the robustness of the model, results for different DEM resolutions, sink-fill depths, and flow accumulation values (described below) are compared. These functions are presently available in ArcGIS 9–Spatial Analyst Extension and Arc/Info.

[19] The approach taken here involves application of techniques used for drainage basin and network analyses on the Earth, where watershed formation is dominated by precipitation, to the surface of Mars. As some of the assumptions may or may not be representative of the Martian case, we evaluate the technique as we seek to learn about the hydrologic history of Tyrrhena Terra. Certain steps involve only use of Martian topography and thus provide reliable quantitative characterization of drainage basins, assuming the effects of impact craters forming after fluvial dissection can be accounted for. Using drainage basins delineated from Martian topography and mapped valley networks, watersheds can be described both qualitatively and quantitatively. Comparison of mapped and model-predicted valley networks (and the derived topologic parameters) reveals similarities and differences between the terrestrial and Martian cases and provides insights into network formation and watershed maturity.

4.1. Data Sets and Hydrologic Mapping

[20] All available (as of September 2004) Viking Orbiter (10–90 m/pixel), THEMIS infrared (day)- and visible (~100 and 20 m/pixel, respectively), and MOC narrow-angle (1–8 m/pixel) and wide-angle (~237 m/pixel) images were used to visually identify valleys and produce a detailed hydrologic map of the Tyrrhena Terra study area on a Mars Digital Image Mosaic (MDIM) version 2.0 base (231 m/pixel) in Adobe Illustrator. The high-resolution image data have allowed significantly more tributaries to be identified than in previous studies [e.g., *Carr and Chuang*, 1997]. In this study, mapped valleys do not include inferred valleys from topography as other investigations have done, in order to avoid misidentifying other features (e.g., crater chains, fractures, etc.) as valleys. The valley map and MDIM base were imported as raster files into ESRI Arc/Info GIS software and converted to arc coverage feature-based and GRID raster-based geodata sets, respectively.

[21] A Digital Elevation Model (DEM) of the study area, generated from gridded MOLA topographic data courtesy of the Planetary Geodynamics Laboratory at Goddard Space Flight Center, was imported into Arc/Info in ASCII format and converted to Arc/Info raster GRID format. The gridding procedure used by the Laboratory is the same as that utilized by the Planetary Data System to generate the Initial Experiment Gridded Data Records (IEGDRs). The DEM used in this project was generated using the equivalent number of MOLA tracks as the IEGDRs, not the Mission Experiment Gridded Data Records. At the time this study was conducted, DEMs were released at 4, 16, 32, and

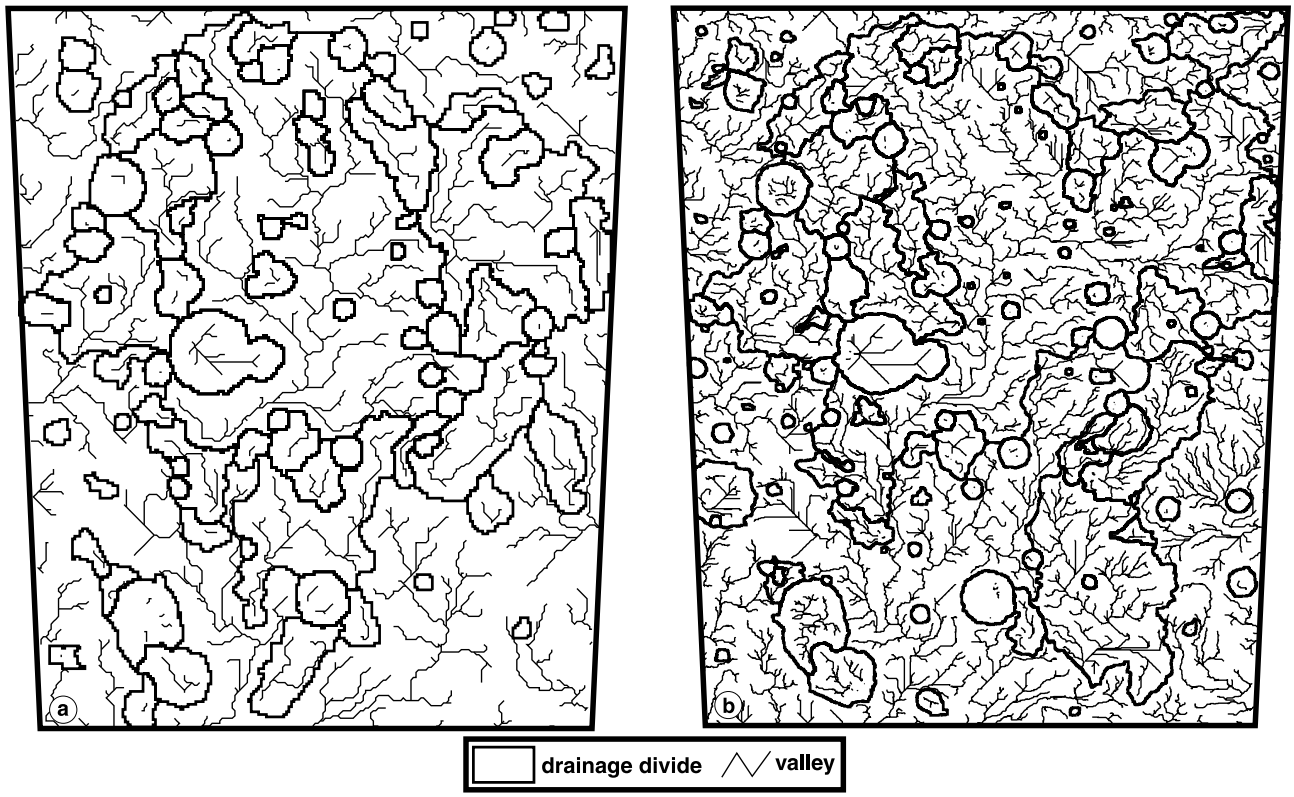

Figure 6. Watersheds in Tyrrhena Terra (13°S to 30°S, 265°W to 280°W) extracted (SFD = 575 m and FAV = 575) using (a) 16 and (b) 64 pixels/degree DEMs. Within the same spatial area, the 64 pixels/degree DEM delineates more drainage basins (151 basins) and valley networks display more tributaries than the 16 pixels/degree DEM (91 basins).

64 pixels/degree; the 128 pixels/degree DEM was not released at the time of this study and was therefore not used.

[22] *Mest et al.* [2001a, 2001b] conducted a comparison study of the 16, 32, and 64 pixels/degree DEMs to test the model against DEM resolution; this type of analysis has been applied in terrestrial hydrologic modeling studies [e.g., *Wang and Yin*, 1998; *Gyasi-Agyei et al.*, 1995; *Kenward et al.*, 2000] and has shown that DEMs with higher spatial and vertical resolution more accurately determine flowpaths within watersheds. The 16 and 64 pixels/degree DEMs both have a vertical resolution of ~10 m [*Smith et al.*, 2001]. Given their spatial and vertical resolutions, both data sets would be expected to most accurately predict features greater than 10 m deep and greater than 4 km (16 pixels/degree) and 1 km (64 pixels/degree) wide. The results of this comparison (Figure 6) show that the 64 pixels/degree DEM, the highest resolution DEM available at the time, yielded the closest results to the mapped valley networks.

[23] All data, MDIM, mapped valleys, and DEMs, were projected into a sinusoidal coordinate system using Mars2001 (IAU2000) as the Martian spheroid, where the semimajor and semiminor axes equal 3,396,190 m (this spheroid is used for all subsequent Martian data layers). Sinusoidal projection was used because it is adequate for small-scale analyses and for low- to midlatitude regions, and it is an equal-area projection, appropriate for calculation of drainage basin areas [*Snyder*, 1982].

4.2. Hydrologic Modeling

[24] Drainage divides and valley networks were derived from standard techniques that have been used to extract terrestrial drainage networks from topographic data sets [e.g., *O'Callaghan and Mark*, 1984; *Jenson*, 1991; *Tarboton et al.*, 1991; *Thieken et al.*, 1999; *Turcotte et al.*, 2001; *Vogt et al.*, 2003]. Four standard surface water hydrologic Arc/Info GRID model functions (FILL, FLOWDIRECTION, WATERSHED, AND FLOWACCUMULATION) were used to derive drainage basin divides and generate valleys from the MOLA DEMs.

[25] The FILL function removes sinks, which here include artifacts from DEM generation, as well as the deepest pixels found within impact craters or other enclosed depressions in the topographic data set. Removal of these pixels considerably improves model results and is a standard step in terrestrial surface water runoff modeling [*O'Callaghan and Mark*, 1984; *Jenson and Domingue*, 1988; *Fairfield and Leymarie*, 1991; *Tarboton et al.*, 1991; *Martz and Garbrecht*, 1998], the purpose of which is to create a depressionless DEM by allowing water to flow along paths that may be interrupted by depressions, such as lakes, or in this case craters. With respect to hydrologic modeling, a sink can be a single pixel or set of spatially connected pixels the drainage direction of which is undefined because all pixels surrounding the sink are higher; thus, water would flow into a sink but would have no point from which to continue flowing downslope. Here

Table 1. Sink Data for 15 Model Runs in Tyrrhena Terra[a]

Mean Accumulation Value	Sink-Fill Depth (m)	Number of Sinks Filled[b]	Percent of Sinks Filled	Percent of Surface Modified
15	0	0	0.0	0.000
152	100	15,900	95.3	0.760
294	323	16,371	98.1	0.783
406	400	16,437	98.5	0.786
410	450	16,461	98.7	0.787
469	500	16,487	98.8	0.788
472	540	16,509	98.9	0.789
492	550	16,514	99.0	0.789
524	560	16,520	99.0	0.790
530	570	16,530	99.1	0.790
575	575	16,533	99.1	0.790
595	580	16,534	99.1	0.790
609	600	16,539	99.1	0.791
646	639	16,553	99.2	0.791
966	960	16,633	99.7	0.795

[a]Tyrrhena Terra DEM (64 pixels/degree) is 2177 rows by 961 columns (2,092,097 pixels).
[b]Total number of sinks identified in the Tyrrhena Terra DEM = 16,682.

less than 1% (16,682) of the total pixels (~2 million) in the DEM were identified as sinks, which is comparable to corrections made to terrestrial DEMS in which 0.9% to 7% of pixels are sinks [*Tarboton et al.*, 1991]; for this study, sinks identified in the MOLA DEM include irregularities (the common source of sinks in terrestrial DEMs), as well as impact craters and other depressions. Sinks are filled to a depth, referred to as the "sink-fill depth" (SFD), which represents the maximum depth of a sink that will be filled. Using the GIS software, all sinks with a depth less than the SFD relative to their lowest adjacent pixel, defined as the pour point (the point where water would continue to flow downslope), are filled to the pour point pixel elevation. Conversely, sinks with a depth greater than the SFD, relative to the pour point, are not filled. In general, filling sinks increases the ability of the DEM to be fully drainable. Table 1 shows the percent of sinks filled for 15 iterations of the model. Part of the extraction technique, described in following sections (e.g., section 4.3), has been to determine the appropriate SFD to delineate drainage basins at a scale adequate to approximate basins identified from mapped valley distributions. In this study, most groups of pixels that were identified as sinks consisted of small craters, most of which postdated the fluvial activity that modified this part of the highlands of Terra Tyrrhena.

[26] The FLOWDIRECTION function creates a grid of flow direction (or slope grid) from each pixel to its steepest downslope neighbor in a 3 × 3 pixel neighborhood [*O'Callaghan and Mark*, 1984; *Jenson and Domingue*, 1988; *Vogt et al.*, 2003]. This function indicates the direction in which surface water will flow from one pixel to another by calculating the direction of steepest descent from each cell.

[27] The WATERSHED function utilizes the FLOWDIRECTION grid and identifies pour points to determine drainage divides. The pour point, which is the lowest point along an entire drainage flow path, is used by Arc/Info to determine the pixels that occur upslope from the pour point to the drainage divide, thus, calculating the contributing area or the areal extent of a drainage basin. In ideal cases, a single pour point is identified at the drainage mouth; in this study, pour points occur on the floors of craters within a drainage basin and along the edge of the DEM. It should be noted that networks that have outlets that occur along the edges of the DEM are not included in our analysis because they are not enclosed by drainage divides within the study area and the valleys may continue beyond the extent of the DEM.

[28] The FLOWACCUMULATION function is used to calculate an accumulation grid, which is a grid of accumulated flow to each "downstream" pixel or simply the area that can potentially produce runoff to a pixel of interest [*Jenson and Domingue*, 1988; *Tarboton et al.*, 1991; *Vogt et al.*, 2003; *Erskine et al.*, 2006]; this value is also referred to as upslope area and contributing area in the literature. Accumulated flow is based upon the number of upstream pixels that contribute to each subsequent downstream pixel. ESRI Arc/Info software uses a flow accumulation threshold method to determine the locations of stream channels. Lowering the flow accumulation value (FAV) results in a corresponding increase in drainage density. The software accumulates the weight for all pixels in the grid that flow into each downslope cell; in general, pixels with zero flow are topographic highs and determined to be the drainage divides, and pixels with high accumulation are areas where water is concentrated and are used to determine the locations of stream channels. Valleys for each run were initially delineated using the mean FAV calculated for each run (see Table 1) that is obtained from the associated ACCUMULATION grid. For example, for SFD = 575 m (see section 4.3 below), the mean FAV is equal to 575 cells, and for a SFD = 100, the mean FAV is 152 cells; thus, any pixels with accumulation values greater than the threshold would be considered to accumulate enough water in order to be delineated as a valley. Ten additional runs were conducted using a SFD = 575 and FAVs between 100 and 5583 (see section 4.4 below) to explore the dependence of extracted networks on FAV and select runs appropriate for analyses of Tyrrhena Terra.

[29] Near-global topographic coverage of Mars by MOLA data and HRSC stereo images [e.g., *Ansan et al.*, 2007] has enabled other researchers to conduct hydrologic modeling studies similar to the one presented here. *Craddock et al.* [2001a, 2001b, 2003] used GIS techniques similar to the current study to extract drainage networks and divides from the MOLA data set and to compare them to mapped valleys between ±30° latitude. Results showed that streams with orders ≤3 were not accurately identified or located, a finding attributed to DEM resolution, but streams with order >3 were more accurately identified. In Terra Cimmeria, a combination of MOLA-derived drainage divides, mapped valleys, and geologic analyses was used to show a complex fluvial history involving competition with impact cratering, breaching of divides, and redirection of flow by large craters [*Irwin and Craddock*, 2001; *Irwin and Howard*, 2002; *Irwin et al.*, 2002a; *Irwin and Maxwell*, 2003].

[30] Other studies have used similar techniques to automatically extract valley networks and drainage divides from topographic data, but these typically do not account for the effects of local and regional geology, as well as the valuable corroborating evidence from image data sets. Some analyses used MOLA DEMs to model drainage basins on a global scale in which Mars was divided into eight [*Banerdt and*

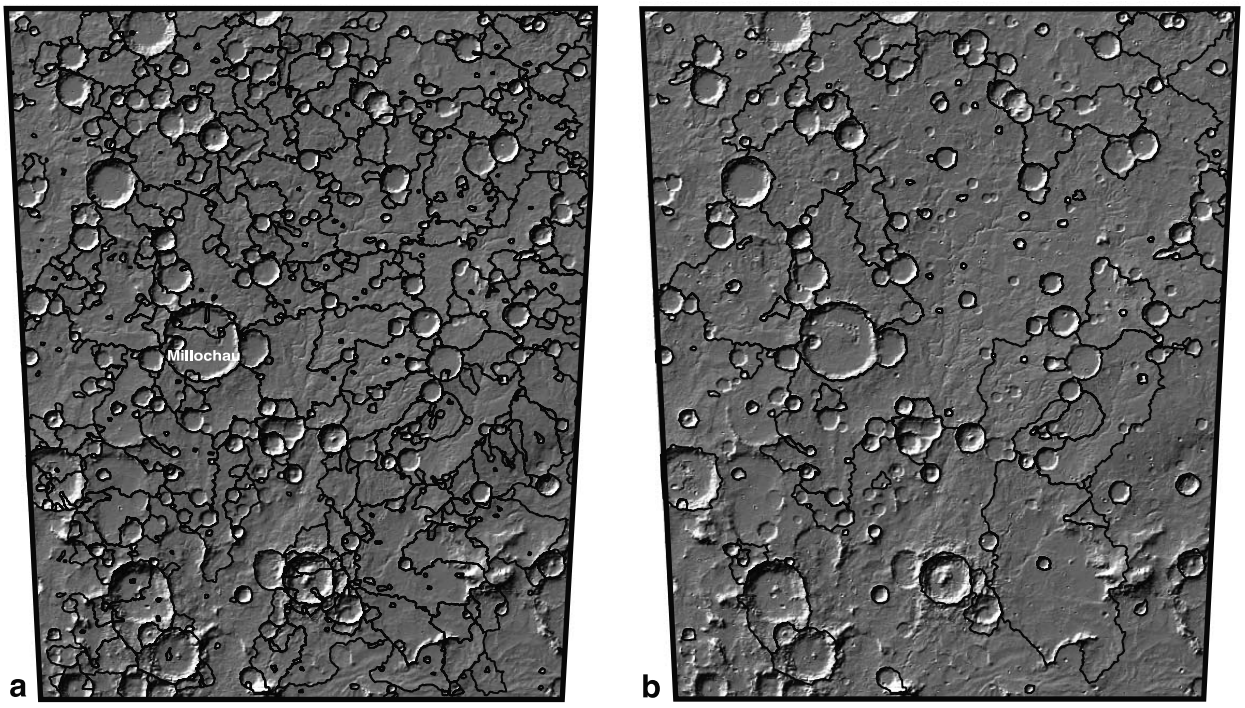

Figure 7. Model-predicted watersheds in the Tyrrhena Terra study area demonstrating the effects of different sink-fill depths on the numbers of watersheds produced and the detail for each network. Here watersheds are extracted for sink-fill depths of (a and b) 100 m and (c and d) 575 m; FAV = 575 for both models. The larger sink-fill depth yields fewer, less detailed watersheds; 784 and 151 basins are generated for SFD = 100 and 575 m, respectively, for the entire region. (a and c) In the regional views, significant watersheds are observed that correlate with impact craters that denote sinks; as watersheds are extracted at higher sink-fill depths, more of these impact-crater-watersheds are eliminated and incorporated into larger systems. (b) In close-up view, many of the larger craters, such as crater Millochau, are subdivided into multiple watersheds.

Vidal, 2001] and eleven [*De Hon*, 2002] regional watersheds. Other studies [e.g., *Stepinski et al.*, 2002a, 2002b, 2003; *Collier et al.*, 2003; *Stepinski*, 2003, *Stepinski and Collier*, 2003, 2004a, 2004b; *Molloy and Stepinski*, 2007] have conducted quantitative analyses of valley networks extracted from MOLA DEMs in an attempt to characterize the processes (runoff versus sapping) responsible for valley formation.

[31] Our approach uses a DEM with filled sinks to determine drainage divides and then a flow accumulation value to determine the locations of fluvial valley segments. Results are compared in a two-step process to the geology of the region using results from detailed mapping. An optimal SFD or range of optimal SFDs is identified on the basis of: (1) the match of predicted drainage divides to the topography of the region, taking into account the potential for impact-generated topography following fluvial incision; and then (2) the match of predicted and mapped valley segments, again with consideration of competition between cratering and fluvial activity. Our overall approach is consistent with a number of terrestrial analyses [e.g., *O'Callaghan and Mark*, 1984; *Jenson and Domingue*, 1988; *Fairfield and Leymarie*, 1991; *Jenson*, 1991; *Tarboton et al.*, 1991; *Martz and Garbrecht*, 1998; *Thieken et al.*, 1999; *Turcotte et al.*, 2001; *Vogt et al.*, 2003]. Recent work, relevant to both the Earth and Mars, involves several different approaches, such as using of the curvature of the surface to define flow direction [e.g., *Luo and Stepinski*, 2009].

4.3. Sink-Fill Depth

[32] A critical step was to determine the sink-fill depth (SFD) that generated drainage divides containing the mapped networks and that produced stream systems approximating the positions of individual valleys and the scales of observed networks. Automatically delineated drainage divides were visually compared to image and topographic data sets, factoring in crater/valley temporal relationships, and to slope maps generated from the MOLA DEM. As mentioned previously, the FILL function increases the ability of the DEM to be fully drainable. Tyrrhena Terra contains numerous impact craters and other depressions that formed subsequent to valley formation and that interrupt continuity of valley networks. Using the FILL function, a SFD can be selected that fills shallower depressions, thus, permitting flow in some areas, while leaving deeper depressions (which usually represent isolated watersheds) unaffected. Use of the raw DEM (i.e., SFD = 0 m, FAV = 14.8 (mean value)) results in identification of over 16,000 small drainage basins that include anomalous pixels, small impact craters, and other surface depressions, yielding a surface and networks that are overly fragmented. Con-

Table 2. Drainage Basin Statistics for 15 Model Runs in Tyrrhena Terra (FAV = 575).

Total Area[a] (km^2)	SFD (m)	Number of Basins[b]	Minimum Area[c] (km^2)	Maximum Area[d] (km^2)	Mean Area[e] (km^2)
819,701.7	0.0	17,737	0.20	1251.4	46.2
667,965.9	100.0	803	0.40	16,397.9	831.8
578,311.9	322.7	319	0.40	90,097.6	1812.9
536,950.8	400.0	251	0.40	128,382.0	2139.3
533,988.2	450.0	227	0.40	131,074.9	2352.4
519,652.9	500.0	200	0.40	146,558.4	2598.3
510,681.3	540.0	177	0.40	152,195.7	2885.5
496,952.8	550.0	171	0.80	152,242.8	2906.2
496,236.7	560.0	165	0.80	170,065.5	3007.5
480,464.7	570.0	155	0.80	170,364.5	3099.8
480,464.7	575.0	151	0.80	177,557.1	3181.9
480,464.7	580.0	150	0.80	177,557.1	3203.1
478,563.2	600.0	145	0.80	180,896.5	3300.4
434,078.3	639.0	130	0.80	215,158.8	3339.1
110,531.2	960.0[f]	50	0.80	17,944.0	2210.6

[a]Sum of the areas of all basin delineated by the algorithm.
[b]Total number of drainage basins delineated by the algorithm.
[c]Area of smallest basin delineated by the algorithm.
[d]Area of largest basin delineated by the algorithm.
[e]Average basin area calculated from the total area/number of basins.
[f]Since the study area has a finite boundary, terrain not enclosed within a drainage divide remains open and any valleys generated will flow toward the artificial edge of the DEM. At SFD = 960 m, we reach this threshold which results in an unenclosed area significantly larger than the largest enclosed drainage basin; thus, the area parameters (total, maximum, and mean) decrease.

versely, completely filling all sinks (SFD = 960 m, FAV = 965.8 (mean value)) results in an uninterrupted, and over-integrated network. Both of these extremes are unrealistic with respect to what is observed in image data. “”Therefore, a sink-fill depth (coupled with a flow accumulation value) must be selected that best approximates the observed watersheds (i.e., drainage basin areas and positions, positions of trunk valleys, scales of networks), taking into account the spatial and temporal relationships between valleys and the impact craters that cause most of the valley disruptions.

[33] A standard procedure for identifying an “optimal” sink-fill depth was used for the first few iterations of the model and included running the FILL function for SFDs equal to 0 (zero) m, the mean sink depth (for the study area), and ±one half the mean. For the 64 pixels/degree DEM, these SFDs were equal to 0.0, 322, 639.4, and 960 m. The resulting watershed and network GRIDs (derived using the mean FAVs from corresponding FLOWACCUMULATION GRIDs shown in Table 1) were overlain on the image-based network map to compare model accuracy. This initial comparison would indicate whether additional iterations of the model were necessary. Two specific criteria were applied to determine which FILL iteration most closely approximated the mapped networks: (1) do the number of delineated drainage basins equal the number of mapped networks and (2) do the delineated drainage divides enclose the mapped networks. For derivation of network morphometric parameters, the optimal SFD is later coupled with an optimal FAV that is selected based on the best match of extracted and mapped valleys (as discussed below). For the 64 pixels/degree DEM, the mapped networks most closely matched the initial 322 m and mean SFD runs. To further assess accuracy, results were generated for several additional sink-fill depths, shown in Table 1. Results for these runs were compared to the mapped networks as described above. It was concluded that the 575 m SFD-generated drainage divides that adequately enclosed mapped networks. This iteration (SFD = 575 m) was selected and coupled with an optimal FAV for characterization of the morphometric parameters of the watersheds of interest.

[34] For watersheds of the scale observed in Tyrrhena Terra and the resolution of the MOLA DEM (64 pixels/degree), results (Table 1) are sensitive to large changes in SFD (>10 m; e.g., SFD = 570 m versus 600 m). Small-scale SFD adjustments (<10 m; e.g., SFD = 570 m versus 575 m versus 580 m) do not significantly change the numbers of drainage basins and the positions of drainage divides. Table 2 shows some of the areal data derived from fourteen iterations with sink-fill depths ranging from 0 to 960 m, and Table 1 shows the percent of sinks filled in the Tyrrhena Terra MOLA DEM. Figure 7 shows differences in the numbers and sizes of drainage basins identified in the Tyrrhena Terra study area and the lengths and morphology of networks predicted by the model. This test shows that increasing the sink-fill depth will yield fewer drainage basins because basins are merged, but with larger areas (Table 2; Figure 7).

[35] Divides for terrestrial drainage basins generally consist of ridges formed tectonically, volcanically, or by continued erosion. However, on Mars, abundant impact craters form effective divides by collecting and distributing water and sediment to crater floors, disrupt drainage patterns, or form drainage basins within drainage basins. Previous researchers have used various techniques to identify Martian drainage divides, including stereo pairs [*Boothroyd and Grant*, 1985; *Grant*, 2000] and the most headward extension of tributaries [*Kochel et al.*, 1985; *Baker and Partridge*, 1986]. Figure 7 shows many of the delineated drainage divides for both sink-fill depths correspond to the locations of impact craters; given our geologic interpretation of the region, which indicates that many craters postdate the main period of fluvial activity [*Mest*, 2004; *Mest and Crown*, 2006], experimenting with different corrections of associated single pixel sink anomalies can provide the most suitable DEM for testing the extraction technique. For this research an ideal sink-fill depth of 575 m is chosen because (1) the resulting divides adequately enclose the mapped networks and (2) this SFD eliminates (or isolates as sub-basins) drainage divides delineated by the rims of single or nested impact craters that postdate the fluvial activity. Selection of this sink-fill depth focuses our analyses on 11 watersheds in Tyrrhena Terra.

4.4. Flow Accumulation Value

[36] The second key parameter, the flow accumulation value, is critical in properly delineating networks. As mentioned previously, the FLOWACCUMULATION function is used to calculate a grid of accumulated flow to each “downstream” pixel. From this grid, valleys can be defined as pixels that exceed an accumulation threshold [*O'Callaghan and Mark*, 1984; *Jenson and Domingue*, 1988; *Mark*, 1988; *Jenson*, 1991; *Tarboton et al.*, 1991; *Soille et al.*, 2003; *Vogt et al.*, 2003], here referred to as the flow accumulation value (FAV). In terrestrial studies, the flow accumulation threshold (or contributing area threshold) is critical in determining channel head location, which

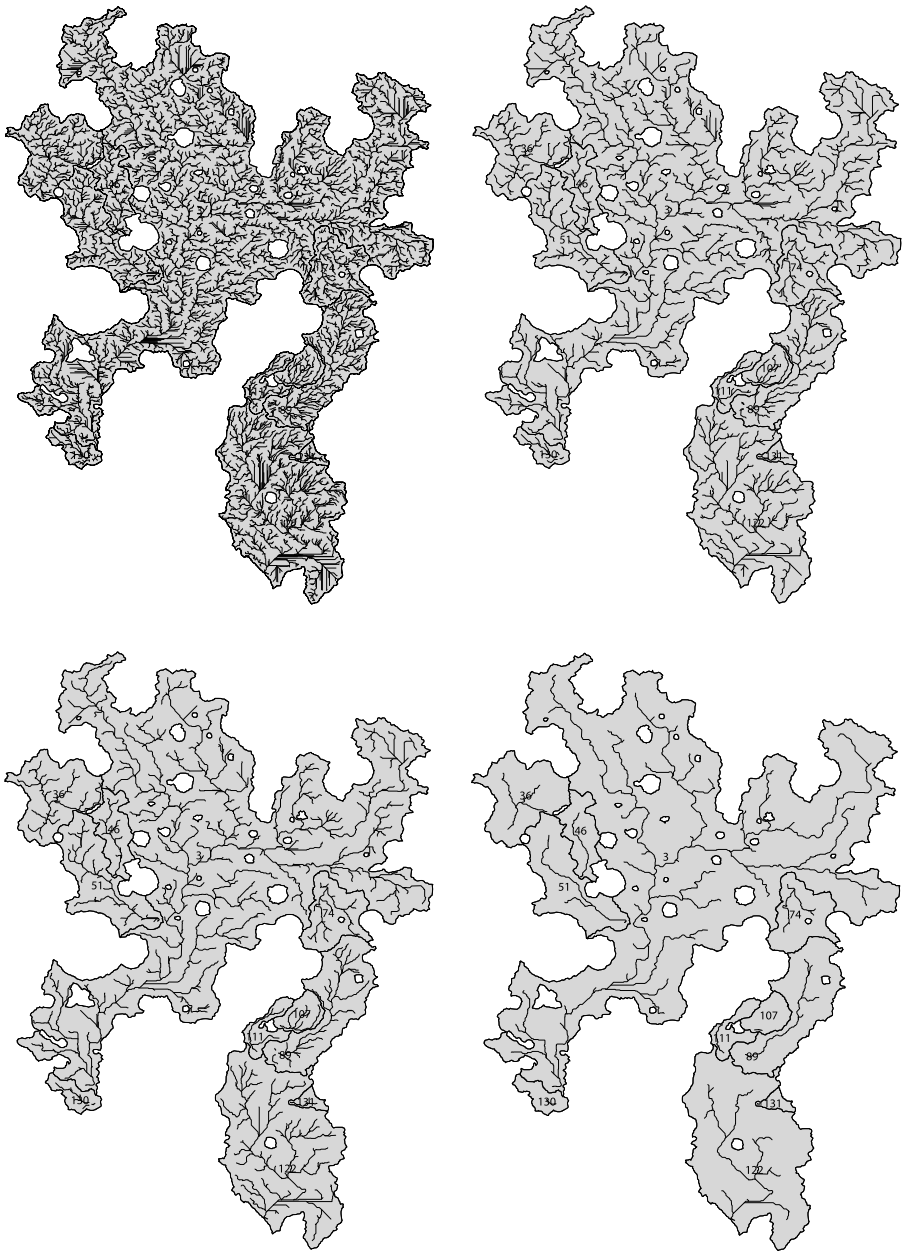

Figure 8. Model-predicted watersheds with SFD = 575 and (a) FAV = 100, (b) FAV = 558, (c) FAV = 1000, and (d) FAV = 5583. Increasing FAV results in fewer streams and increased lengths between stream junctions for higher-order streams.

generally corresponds to areas where fluvial transport overcomes diffusive transport and slope transition from convex to concave [*Vogt et al.*, 2003 and references therein].

[37] As noted in many terrestrial watershed studies [e.g., *O'Callaghan and Mark*, 1984; *Jenson and Domingue*, 1988; *Mark*, 1988; *Jenson*, 1991; *Wang and Yin*, 1998; *Soille et al.*, 2003] and similar to alterations in the sink-fill depth with respect to drainage basin delineation, lowering the FAV in the model results in a corresponding increase in drainage density. As Table 3 and Figure 8 show, a FAV = 100 results in networks with high drainage densities, whereas a FAV = 5583 results in networks with significantly lower drainage densities. Both of these extremes, when compared with the mapped networks, are unrealistic, and it is therefore necessary to select an FAV or FAVs that will best approximate the observed networks (using the previously determined 575 m SFD as the optimal representation of drainage basins).

[38] The procedure for selecting a FAV is similar to that of the SFD. The runs for selecting the "ideal" SFD, which utilized the mean FAVs for corresponding ACCUMULATION grids, provided the basis for testing and selecting the "ideal" FAVs for each basin. Generally, low FAVs yield too may valleys and high FAVs produce too few valleys. Two of the initial FAVs tested, 100 and 558 (Figure 8), were similar to values used in the SFD analysis; the other two FAVs tested, 1000 and 5583 (Figure 8), are an order of magnitude greater and were selected for comparison with

Table 3. Flow Accumulation Value Data for 10 Model Runs in Tyrrhena Terra[a]

FAV	Number of Streams[b]	Total L[c] (km)	Minimum L[d] (km)	Maximum L[e] (km)	Mean L[f] (km)	Standard Deviation[g] (km)	D_d[h] (km^{-1})
100	5156	49,347	0.3	717	10	18	0.169
190	2739	35,529	0.2	717	13	23	0.122
279	1892	29,396	0.4	717	16	27	0.101
400	1300	24,581	0.3	717	19	31	0.084
558	957	20,967	0.2	717	22	35	0.072
575	933	20,684	0.7	717	22	35	0.071
667	832	19,312	0.6	716	23	37	0.066
775	721	17,826	0.6	717	25	41	0.061
1000	563	15,785	0.6	717	28	45	0.054
2000	284	11,060	0.3	846	39	67	0.038
5583	102	6637	2.1	565	65	85	0.023
Mapped	599	8701	0.7	316	15	23	0.030

[a]Data compiled from 11 drainage basins identified in Tyrrhena Terra using SFD = 575 m.
[b]Total number of streams.
[c]Sum of the lengths of all streams delineated by the algorithm; only streams enclosed within a drainage basin are summed.
[d]Length of shortest stream.
[e]Length of longest stream.
[f]Average stream length, calculated from the total length/number of streams.
[g]Standard deviation of the mean stream length.
[h]D_d (drainage density) = total L/drainage basin area.

basins with few mapped valleys. The resulting networks from these four iterations were compared to the image-based mapped networks. The two main criteria used to determine which iteration most closely approximated the mapped networks are valley placement and valley numbers. Are the locations of the valley heads and along stream portions of the extracted valleys equivalent to the mapped valleys, and are the numbers of the extracted valleys roughly equivalent to the mapped valleys? Analysis of these results determined whether additional iterations were necessary. However, unlike selection of an ideal SFD, it was observed that selection of an ideal FAV is more complicated and is a basin-dependant value due to the inconsistencies in topography and geology from basin to basin. *Vogt et al.* [2003] noted most models apply a single threshold over large areas, which requires a relatively homogeneous landscape; however, for networks developed on heterogeneous landscapes (such as on Mars), it is more appropriate to apply different thresholds or variable thresholds (e.g., slope-dependent) to account for these variations.

[39] Figure 9 provides examples that show the complexity in selecting FAVs for individual Tyrrhena Terra basins; accurately identifying FAVs for regional scale applications can be difficult without detailed geologic constraints. Basin #51 (Figure 9a) appears to be best approximated by a FAV = 2000; with the exception of the lack of valleys mapped in the northern part of basin #51, the locations of valley heads and the numbers of tributaries appear equivalent, and this is supported by additional length data shown in Table 4a. Conversely, basin #89 (Figures 9b and 10c) displays steeper topography (from impact craters) and higher drainage densities in the western and southern parts of the basin than in the eastern part. “”Here variations in topography may have contributed to variations in drainage density, and a variable FAV is appropriate. As shown in Figure 9b, a visual comparison shows the FAVs that “best fit” the mapped network in basin #89 are equal to 100 for the western and southern parts of the network and 775 for the eastern part, but for the purposes of this work, an FAV of 775 is selected for basin 89 because it is consistent with most of the other watersheds that closely match models with high (>1000) FAVs (Table 4b). In a simple case (i.e., homogeneous landscape), a single regional flow accumulation value would be chosen that approximates the overall locations of all mapped networks, as well as approximating smaller-scale network features, such as the numbers and positions of tributaries. However, because of the complexity of the landscape, individual FAVs are selected for each of the 11 basins identified in the Tyrrhena Terra study area (Table 7b).

5. Results

[40] The following results are based on (a) valley networks mapped from image data sets and (b) basin divides and networks generated using a SFD = 575 m, FAV values shown in Table 7b, and a 64 pixels/degree MOLA DEM. Analysis of zonal elevation statistics associated with single or multiple pixel sinks identified 0.79% (16,682 pixels) of the DEM (~2 million pixels) as having undefined surface water flow directions (Table 1). Modeling at SFD = 575 m yielded 151 drainage basins and several networks with no associated divides that extend beyond the limits of the study area. Image analysis shows that drainage divides consist of combinations of impact crater rims, ridges, and knobs associated with upland terrains and other ridge-forming structures. Of the 151 basins, 119 correspond to impact craters (79%), of which 111 are single craters (93%) and 8 are clusters of two or more craters (7%). Of the 119 crater basins, 58 of these (49%) correspond to impact craters (single and clusters) that postdate fluvial activity in Tyrrhena Terra (56 are single craters and 2 correspond to clusters (1 doublet and 1 triplet cluster), of which only one crater in each cluster postdates fluvial activity).

[41] Mapped and extracted networks were rigorously compared to test the validity of the modeling technique and for analysis of watershed formation. The results discussed here focus on 11 basins (Figure 10a) that adequately encompass the mapped networks shown in Figure 10b.

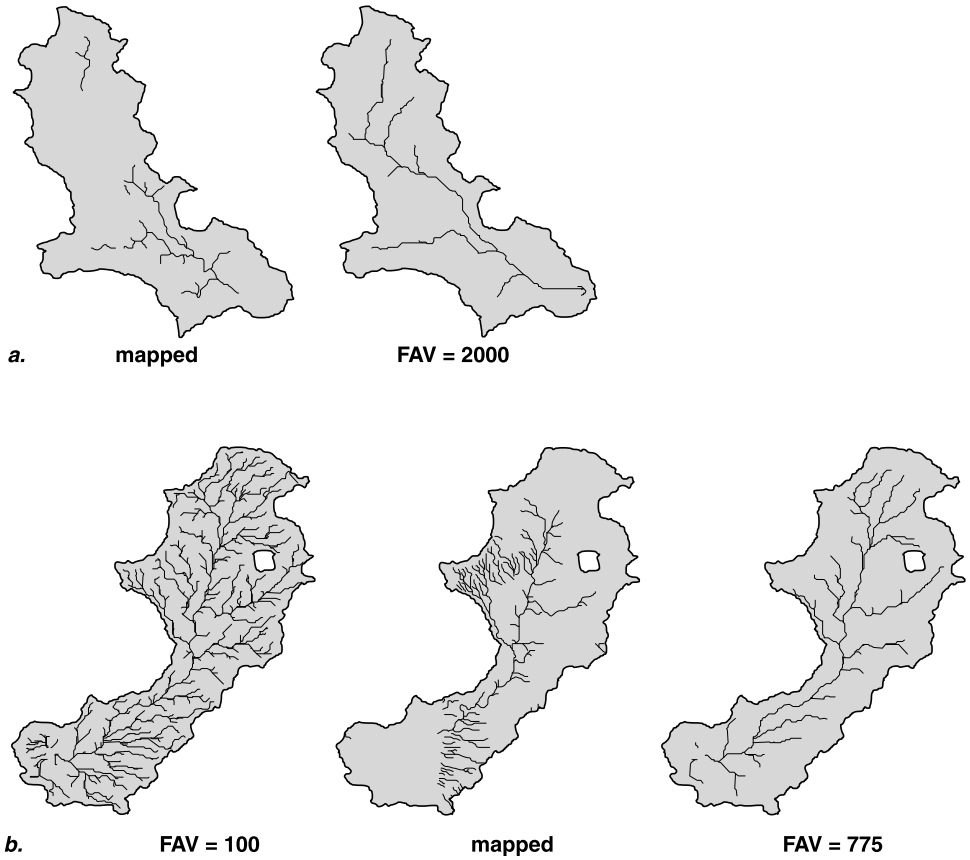

Figure 9. Close-up comparison of mapped networks and closest-match extracted watersheds for basins (a) 51 and (b) 89. (a) Basin 51 shows a closest match for FAV = 2000 despite the large area devoid of networks in the mapped watershed. (b) More complex watersheds, such as 89, show higher drainage densities on steeper slopes and lower densities in flatter terrain in the mapped watershed. FAV = 100 best approximates the denser networks in the northwest part of this watershed, and FAV = 775 best approximates the networks formed in the flatter terrain in the east and southeast parts of this watershed. Extracted networks calculated with SFD = 575.

Morphometric parameters (Table 5) were calculated for both mapped and extracted networks. These parameters are valuable in geomorphic analysis and classification of drainage basins and have been used to relate the measurable properties of terrestrial drainage basins to geology and streamflow patterns [*Horton*, 1932, 1945; *Strahler*, 1957, 1958, 1964; *Gregory and Walling*, 1973; *Baker and Partridge*, 1986], as well as climate and precipitation patterns [*Gregory*, 1976; *Gyasi-Agyei et al.*, 1995; *Ritter et al.*, 1995; *Vogt et al.*, 2003].

5.1. Comparison of Mapped and Model-Predicted Watersheds

[42] Visual inspection of mapped and extracted watersheds for the 11 selected basins shows an overall good match for the locations of valley networks but an overall poor match for the amount of dissection and the drainage density. Regional differences between mapped and extracted networks can be seen in Figures 10a and 10b, and a specific comparison is shown in Figures 10c and 10d for basin #89. Higher-order (second- and third-order) extracted valleys are good approximations of the equivalent mapped valleys in terms of both the numbers and locations of valleys, but the numbers and locations of extracted valleys are less accurately predicted for first-order tributaries. In basin #89 (Figure 10c), third- and fourth-order mapped valleys correspond well with second- and third-order extracted valleys that occur on the lowest slopes (0.2°–0.4°) within this basin. However, first-order extracted valleys in basin #89 rarely have a corresponding mapped valley, which tend to occur on the steeper slopes in the basin, and do not have the same density as the mapped valleys, as shown in Figure 9. The coarseness of the MOLA DEM, as well as the method chosen to valleys (with dependencies on values of sink-fill depth and flow accumulation threshold) have an effect on delineation of the more closely spaced parallel valleys observed on the steeper slopes of basin #89. MOLA spatial resolution (~460 m/pixel) does not allow delineation of valleys in areas where their spacing is on the order of ≈tens of meters, as observed on the steeper slopes of basin #89. The iterative process for selecting the FAV and the reasonable match for lower-order mapped and modeled valleys suggests that either this approach needs additional constraints on the surface geology, that a variable intrabasin FAV is needed, and (or) that there are differences in watershed formation between Earth and Mars resulting in less dissection of the Martian surface.

Table 4a. Length Data for Watershed 51 (Area = 14,557 km^2; SFD = 575)

	Number of Streams[a]					Stream Length[b] (km)										
FAV	Total	1st	2nd	3rd	4th	Total	Mean	1st Total	1st Average	2nd Total	2nd Average	3rd Total	3rd Average	4th Total	4th Average	D_d[c] (km^{-1})
100	246	194	43	8	1	2302	9	1,214	6	588	14	305	38	195	195	0.158
190	237	107	24	5	1	1665	12	906	9	410	17	153	31	196	196	0.114
279	84	62	18	3	1	1365	16	744	12	290	16	259	86	73	73	0.094
400	65	49	12	3	1	1173	18	636	13	208	17	256	85	73	73	0.081
558	54	42	9	2	1	1023	19	525	13	245	27	181	91	73	73	0.070
575	53	41	9	2	1	1001	19	503	12	245	27	181	91	73	73	0.069
667	48	37	8	2	1	923	19	485	13	184	23	181	91	73	73	0.063
775	37	29	5	2	1	854	23	511	18	138	28	132	66	73	73	0.059
1000	34	26	5	2	1	758	22	420	16	133	27	132	66	73	73	0.052
2000	15	12	2	1	-	456	33	145	12	238	119	73	73	-	-	0.031
5583	3	2	1	-	-	307	102	235	117	73	73	-	-	-	-	0.021
Mapped	23	18	4	1	-	386	17	175	10	166	42	45	45	-	-	0.027

[a]Values shown are for total and as a function of Strahler order.
[b]Values shown are for total, mean, and as a function of Strahler order.
[c]D_d = Drainage density.

[43] Drainage patterns are generally consistent between the modeled and mapped data (Figure 10a and 10b). Mapped networks in Tyrrhena Terra consistently show dendritic (e.g., basin #3) and (sub)parallel (e.g., basin #89) patterns, but the mapped networks within some basins (e.g., basin #3) appear less integrated than the corresponding extracted networks. Subparallel patterns are favored on steeper slopes. Regional slopes in the study area are low (0.23°), which is consistent with the large dendritic pattern of the Vichada Valles system. At smaller scales, steeper, local slopes, such as along the rims of impact craters, produce (sub)parallel drainage patterns. Variations in the geology (lithology, structure, etc.) of the substrate in which valleys are incised could have also influenced drainage patterns. For example, basin #3, which drains the greatest area of the 11 basins identified, contains valleys that dissect a large portion of the intercrater plains [*Mest and Crown*, 2006]. Spatial variations in these layered sequences might influence infiltration and thus the amount of runoff produced [*Ritter et al.*, 1995]. An area overlain by brecciated and fractured (and therefore relatively porous) impact ejecta could have higher infiltration, lower runoff, and thus less dissection than loosely consolidated sediments overlying bedrock [*Kelson and Wells*, 1989; *Ritter et al.*, 1995]. The latter would tend to promote continued headward and lateral growth of channels, as well as initiation of new tributaries as channels erode down to the resistant bedrock and under these circumstances would tend to form networks with dendritic properties.

[44] Combined effects on network morphology by local slopes and lithology can be observed in basins #51 and #89 (Figures 9a and 9b). Basin #51 (Figure 9a), which is bounded by highly degraded impact craters that predate emplacement of the local plains material [*Mest and Crown*, 2006], displays dendritic network morphology (few widely spaced tributaries with broad junction angles), the formation of which is consistent with the low slopes and nature of the plains (loosely consolidated sediments interlayered with ejecta). Alternatively, basin #89 (Figure 9b) is bounded by degraded impact craters in the north and the floor of the basin is covered partially by their ejecta and partially by local plains. The dense network of parallel channels displayed in the northern part of basin #89 is consistent with formation on steep slopes and possibly relatively porous materials, whereas the more dendritic patterns in the southern part of the basin are consistent with formation on lower slopes and possibly more loosely consolidated material.

[45] The surface water hydrologic modeling functions, and similar functions in other hydrologic modeling algorithms (e.g., RiverTools distributed by IDL), use surface water flow on a given DEM to determine watershed geometry and flow networks. As a result, valleys tend to be delineated uniformly across the surface, where the local topography is sufficient to concentrate flow. For modeling of typically precipitation-dominated terrestrial systems, this is appropriate because a fluvial valley is (or was) most likely present. Comparisons of mapped and model-predicted networks on the Martian surface may shed light on the nature of the network-forming processes and the climatic conditions under which they formed (see section 6), although this approach is complicated by several factors. First, high-resolution image data coverage is not consistent across Mars and unless various spacecraft parameters are ideal (sun angle, etc.), visual inspection of images does not always provide a reliable check on extracted valley networks. Given the coarse nature of the MOLA DEM, a variety of geologic and geomorphic features (e.g., graben, crater and pit chains, coalescing ejecta blankets, and debris aprons) can also be misidentified as fluvial valleys. In addition, there is a significant population of impact craters that superpose the surface modified by older fluvial processes; valley-forming processes appear not to have persisted long enough to effectively erode these younger parts of the highlands, a situation different than for many terrestrial applications in which the fluvial activity is current. In this study, we observe differences between the mapped and modeled data sets and we use both mapped and extracted valleys to derive morphometric parameters for comparison and characterization of watersheds in the Tyrrhena Terra region. In regions for which we have good confidence in our ability to reconstruct fluvial systems from photogeologic and topographic analyses, differences in network patterns, integration, and degree of dissection between mapped and model-predicted systems

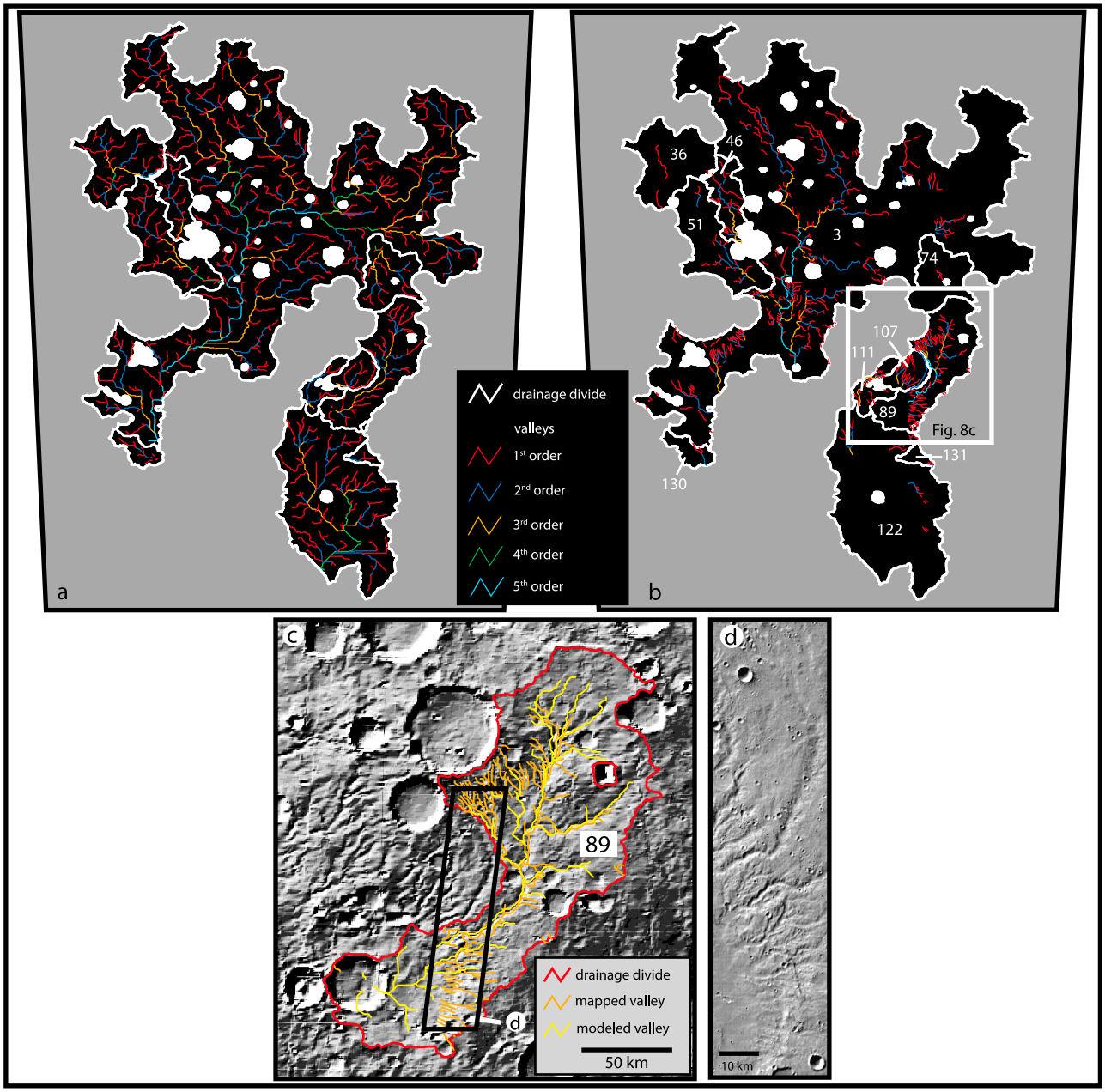

Figure 10. Comparison of extracted (a; SFD = 575 m; FAV = 775) and mapped (b) watersheds for 11 drainage basins (labeled) that are believed to compose the Vichada Valles system; drainage basins within the 11 are shown for reference but are not labeled. The algorithm produces significantly more networks than are mapped from Viking Orbiter, MOC, and THEMIS images. Drainage basins display a range of sizes and shapes, including circular (#107), elongate (e.g., #s 46, 51, and 89), and irregular (#3). Networks are shown as a function of Strahler stream order. (c) Drainage basin #89 and associated extracted and mapped networks; MOLA shaded relief base (centered at 23.0°S, 268.2°W; illumination angle = 40°, azimuth = 30°). The positions of most mapped and extracted trunk valleys in basin #89 are in agreement, as are most of the next lower-order tributaries; however, this iteration of the algorithm does not identify most of the first- and second-order mapped tributaries. Numerous first-order valleys in basin #89 are incised along the rim of a degraded and filled impact crater and terminate on the floor of this crater, (d) as seen in THEMIS daytime infrared image I03680002 (image width ~31 km; resolution ~99 m/pixel; illumination from upper left). The extracted trunk valley in basin #89 continues across the floor of the degraded crater, joining with several tributaries, and terminating on the floor of an ~32 km diameter crater. No valleys are visible on the floor of the degraded crater, and the 32 km diameter crater displays no visible breach in its rim as the algorithm suggests.

Table 4b. Length Data for Watershed 89 (Area = 17,107 km^2; SFD = 575)

	Number of Streams[a]						Stream Length[b] (km)												
FAV	Total	1st	2nd	3rd	4th	5th	Total	Mean	1st Total	1st Average	2nd Total	2nd Average	3rd Total	3rd Average	4th Total	4th Average	5th Total	5th Average	D_d^3 (km^{-1})
100	309	232	59	15	2	1	3012	10	1550	7	894	15	303	20	53	27	212	212	0.176
190	168	127	31	9	1	-	2258	13	1233	10	636	21	177	20	212	212	-	-	0.132
279	108	80	22	5	1	-	1879	17	1113	14	409	19	144	29	212	212	-	-	0.110
400	90	67	18	4	1	-	1594	18	938	14	337	19	108	27	212	212	-	-	0.093
558	66	53	12	1	-	-	1290	20	743	14	317	26	230	230	-	-	-	-	0.075
575	62	50	11	1	-	-	1263	20	726	15	325	30	212	212	-	-	-	-	0.074
667	49	38	10	1	-	-	1148	23	685	18	251	25	212	212	-	-	-	-	0.067
775	46	35	10	1	-	-	1054	23	609	17	232	23	212	212	-	-	-	-	0.062
1000	36	27	8	1	-	-	928	26	545	20	171	21	212	212	-	-	-	-	0.054
2000	16	15	1	-	-	-	548	34	318	21	230	230	-	-	-	-	-	-	0.032
5583	6	5	1	-	-	-	311	52	100	20	212	212	-	-	-	-	-	-	0.018
Mapped	121	96	21	3	1	-	1265	11	790	8	221	11	126	42	128	128	-	-	0.074

[a]Values shown are for total and as a function of Strahler order.
[b]Values shown are for total, mean, and as a function of Strahler order.
[c]D_d = Drainage density.

provide useful insights into subsurface geology and surface processes.

5.2. Impact Crater-Derived Topographic Effects on Hydrology

[46] Impact craters are the dominant local topographic features in Tyrrhena Terra. In order to properly interpret network and basin morphometric parameters, temporal relationships between impact cratering and fluvial activity within the 11 identified drainage basins was assessed. Each basin was categorized according to the relative amounts of cratering that occurred prior to and following fluvial activity. This categorization is used to evaluate the degree of topographic change within a basin relative to the timing of fluvial activity. For example, a significant amount of impact cratering following the main period of fluvial activity within a particular basin would produce topographic changes unaffected by fluvial erosion; in this case, hydrologic modeling could yield vastly different results than for the surface that was subjected to fluvial dissection. In order to assess the relative effect pre- and postfluvial impact craters have on topography and network development, crater size must also be considered. Impact craters identified within the 11 basins are grouped into D > 3 and D > 10 km bins (Table 6), including only craters the rims of which are contained entirely within the drainage divides and do not form any parts of the divides. Craters the rims of which form part of the drainage divide were not selected because their topographic signatures have already been recognized by the model and will affect the locations of delineated valleys. The topographic effects of craters with D < 3 km are believed to be insignificant for the current study. These small-diameter craters would generally not hinder valley development, and valleys could easily adjust their pathways around them. *Hartmann* [1971] showed that early in Mars' history craters with diameters less than ~3 km could be removed from the geologic record in about 100 billion years by burial and erosion, an order of magnitude less than for larger craters, which are more persistent and could thus significantly influence valley development.

[47] Table 6 shows the number and relative percentages of craters greater than 3 and 10 km in diameter that pre- and postdate the main period of fluvial activity (PrFC and PoFC, respectively) for each of the 11 basins. For craters with D > 3 km, five basins contain more PrFCs than PoFCs, four basins show the opposite relationship, and three basins show equivalent numbers of PrFCs and PoFCs. For craters with D > 10 km, five basins contain significantly more PrFCs than PoFCs. Basins 46, 51, 111, 130, and 131 contain no craters larger than 10 km in diameter. Six basins (3, 36,

Table 5. Hydrologic Morphometric Parameters Used in This Study

Parameter	Units	Symbol	Relationship	Reference
Stream order		u		*Strahler*, 1952, 1954
Number of streams of order u		N_u		*Strahler*, 1952, 1954
Stream length	km	L		
Bifurcation ratio (per stream order)		R_b	N_u/N_{u+1}	*Horton*, 1945; *Strahler*, 1952, 1954; *Ritter et al.*, 1995
Bifurcation ratio (for watershed)		R_{bW}	Average of R_b	*Ritter et al.*, 1995
Drainage basin area	km^2	A		
Drainage density	km^{-1}	D_d	$\Sigma L/A$	*Horton*, 1945
Maximum basin relief	m	H	Maximum basin elevation – minimum basin elevation	*Strahler*, 1952; *Schumm*, 1956
Basin length	km	L_b		
Relief ratio		R_h	H/L_b	*Schumm*, 1956
Ruggedness number		R	$H \times D_d$	*Melton*, 1957; *Strahler*, 1958, 1964

Table 6. Distribution of Impact Craters Within 11 Tyrrhena Terra Watersheds[a]

Basin ID	Prefluvial Craters (PrFC)		Postfluvial Craters (PoFC)		Total Craters (PrFC + PoFC)		% PrFC		% PoFC	
	D > 3 km	D > 10 km	D > 3 km	D > 10 km	D > 3 km	D > 10 km	D > 3 km	D > 10 km	D > 3 km	D > 10 km
3	56	30	46	4	102	34	55	88	45	12
36	6	1	4	0	10	1	60	0	40	0
46	1	0	1	0	2	0	50	0	50	0
51	1	0	6	0	7	0	14	0	86	0
74	2	1	4	0	6	1	33	100	67	0
89	7	2	3	1	10	3	70	67	30	33
107	2	1	1	0	3	1	67	100	33	0
111	0	0	2	0	2	0	0	0	100	0
122	8	3	8	1	16	4	50	75	50	25
130	0	0	1	0	1	0	0	0	100	0
131	1	0	0	0	1	0	100	0	0	0

[a]Includes craters that are enclosed entirely within a drainage divide and do not form part of the drainage divide.

46, 89, 107, and 122) show equivalent or less modification by PoFCs. Finally, only basins 3, 89, and 122 contain craters larger than 10 km in diameter (4, 1, and 1 craters, respectively), suggesting only these basins have topography that has been significantly modified by PoFCs, which would affect the results of the Arc/Info model. In Tables 7 and 8, basins 3, 89, and 122 are separated from the other basins (by a double line) to show differences between the morphometric properties of these basins and the other 10 basins. However, it can be seen that the morphometric characterizations of basins 3, 89, and 122 do not differ significantly from other basins in which prefluvial craters dominate the topography.

[48] All of the mapped valleys in basin #89 clearly postdate the surface materials in which they occur (Figure 10c), that is none of the valleys appear to be mantled by impact ejecta or other deposits, and all of the larger craters (D > 10 km) found within basin #89 and those that form portions of the drainage divide clearly predate valley formation. Conversely, in basin #3 (Figure 10a), many of the extracted valleys do not reflect observed crosscutting relationships with craters, but the algorithm predicts valleys where they are not observed in order to form a continuous system around topographic obstructions. For example, the fourth-order mapped trunk valley of Vichada Valles in basin #3 is clearly truncated by a cluster of at least 16 large (D > 10 km) craters (Figures 1 and 11). Seven of these craters (A, D, G, J, K, P, and O in Figure 11) appear to postdate fluvial activity. Given the location and orientation of Vichada Valles at the point of its truncation, only craters J (D ~8 km), K (D ~36 km), and

Table 7a. Length and Area Morphometric Data for Mapped Watersheds

Basin ID	A (km^2)	N	Total L (km)	Minimum L (km)	Maximum L (km)	Mean L (km)	σ (km)	D_d (km^{-1})	u	N_u	Total L_u (km)	Min L_u (km)	Max L_u (km)	Mean L_u (km)	σ_u (km)	R_{bW}
131	1217	5	31	5	10	6	2	0.025	1	4	25	5	10	6	2	4.0
									2	1	6	6	6	6	-	
130	2752	3	60	14	25	20	6	0.022	1	2	35	14	21	17	5	2.0
									2	1	25	25	25	25	-	
111	3401	23	245	1	79	11	16	0.072	1	19	141	1	25	7	6	4.7
									2	3	25	6	12	8	3	
									3	1	79	79	79	79	-	
107	3480	32	424	1	86	13	15	0.122	1	24	258	1	30	11	7	3.5
									2	6	141	3	86	24	32	
									3	2	24	8	16	12	6	
46	6070	18	456	7	83	25	22	0.075	1	14	264	7	49	19	12	3.9
									2	3	108	17	73	36	32	
									3	1	83	83	83	83	-	
74	9016	4	33	2	17	8	6	0.004	1	3	31	5	17	10	6	3.0
									2	1	2	2	2	2	-	
36	13,902	3	119	8	75	40	34	0.009	1	3	119	8	75	40	34	
51	14,557	23	386	4	68	17	16	0.027	1	18	175	4	19	10	4	4.3
									2	4	166	22	68	42	22	
									3	1	45	45	45	45	-	
89[a]	17,107	121	1265	1	128	11	14	0.074	1	96	790	1	27	8	5	4.9
									2	21	221	2	42	11	10	
									3	3	126	25	74	42	28	
									4	1	128	128	128	128	-	
122[a]	43,039	33	396	2	47	12	12	0.009	1	27	239	2	36	9	8	5.2
									2	5	144	3	47	29	17	
									3	1	13	13	13	13	-	
3[a]	177,561	334	5287	1	316	16	27	0.030	1	279	3,085	1	82	11	12	6.7
									2	45	1293	1	151	29	38	
									3	9	593	10	129	66	43	
									4	1	316	316	316	316	-	

[a]These basins contain impact craters (D > 10 km) that are post-fluvial.

Table 7b. Length and Area Morphometric Data for Extracted Watersheds (SFD = 575)

Basin ID	A (km^2)	FAV	N	Total L (km)	Minimum L (km)	Maximum L (km)	Mean (km)	σ (km)	D_d (km^{-1})	u	N_u	Total L_u (km)	Minimum L_u (km)	Maximum L_u (km)	Mean L_u (km)	σ_u (km)	R_{bW}
131	1217	2000	1	38	38	38	38	-	0.031	1	1	38	38	38	38	-	
130	2752	2000	1	64	64	64	64	-	0.023	1	1	64	64	64	64	-	
111	3401	558	9	229	5	75	26	25	0.067	1	6	82	5	31	14	11	2.5
										2	2	131	56	75	65	13	
										3	1	16	16	16	16	-	
107	3480	190	33	428	3	92	13	17	0.123	1	21	140	1	21	7	7	2.7
										2	8	207	2	92	26	28	
										3	3	72	5	39	24	17	
										4	1	9	9	9	9	-	
46	6070	400	25	464	2	143	19	28	0.076	1	20	277	4	43	14	10	4.5
										2	4	44	2	19	11	9	
										3	1	143	143	143	143	-	
74	9016	5583	7	193	3	78	28	27	0.021	1	4	47	3	19	12	7	2.0
										2	2	128	49	78	64	20	
										3	1	18	18	18	18	-	
36	13,902	5583	5	215	13	72	47	22	0.015	1	4	186	13	72	47	25	4.0
										2	1	47	47	47	47	-	
51	14,557	2000	15	456	1	181	33	46	0.031	1	12	145	1	25	12	8	4.0
										2	2	238	57	181	118	88	
										3	1	73	73	73	73	-	
89[a]	17,107	775	46	1054	1	212	23	32	0.062	1	35	609	1	55	17	14	6.8
										2	10	232	1	39	23	14	
										3	1	212	212	212	212	-	
122[a]	43,039	2000	46	1639	1	136	36	32	0.038	1	35	927	2	87	27	22	3.5
										2	8	384	1	102	48	34	
										3	2	193	76	117	96	29	
										4	1	136	136	136	136	-	
3[a]	177,561	1000	322	9627	1	717	30	54	0.054	1	249	4763	1	109	19	16	4.0
										2	56	1814	1	96	34	29	
										3	13	1795	14	357	138	102	
										4	3	438	129	167	146	19	
										5	1	717	717	717	717	-	

possibly P (D ~24 km) were likely involved in its truncation. The path that Vichada Valles took beyond this truncation point prior to emplacement of craters J, K, and P is unclear. Although no distinct valleys remain as evidence for a southern extension of Vichada Valles, due to destruction and (or) burial by craters J, K, P, and crater Isil (south of Figure 11), as well as burial by widespread eolian deposits [*Mest and Crown*, 2001a], several subtle scarp-bounded troughs have been identified within the ejecta of crater K [*Mest and Crown*, 2006]. The algorithm predicted valleys within these troughs (Figure 11). However, it should be noted that predictions of other valleys within the ejecta of craters J, K, P, and Isil are likely to be inaccurate due to the emplacement of these craters after the main period of fluvial activity. Model results show the trunk valley of Vichada Valles extending around the western margin of the cluster of craters, and delineate valleys within the ejecta of some of the craters that clearly postdate fluvial activity in this area. Not only do the image data sets show no evidence for diversion of Vichada Valles, but there also is no evidence for ponding of water north of these craters, suggesting fluvial activity for the most part had ceased prior to formation of craters J, K, and P. Crater O, along the eastern edge of Figure 11, appears to have truncated the mapped valleys in basin #111, and the extracted valleys terminate on the floor of crater O. The remaining craters in this cluster (B, C, E, F, H, I, L, M, and N) appear to predate fluvial activity and have had no effect on Vichada Valles after its course had been established. For this and other parts of the study area, knowledge of temporal relationships between fluvial activity and cratering is critical, and the algorithm alone cannot be accurately used to evaluate Martian valley network development.

5.3. Drainage Density

[49] Drainage density (D_d), defined as the total length of streams in a drainage basin divided by the area of the basin [*Horton*, 1945], is one of the most important morphometric parameters used to characterize valley network development and describes the degree to which a surface is dissected. Terrestrial drainage densities reflect the interaction between geology and climate and are a complex function of relief, slope, lithology, infiltration, total annual precipitation, the ratio of precipitation to evaporation, and vegetation cover [*Horton*, 1932, 1945; *Strahler*, 1952, 1957, 1958; *Gregory and Walling*, 1973; *Ritter et al.*, 1995; *Tucker and Bras*, 1998; *Vogt et al.*, 2003]. In humid and arid climates, low drainage densities are observed when the surface materials are resistant to erosion or have high infiltration capacities. Conversely, high drainage densities can be obtained under either climatic condition as resistance decreases or permeability decreases [*Ritter et al.*, 1995]. All of the above parameters, with the exception of vegetation cover, are applicable to Mars, and only relief and slope can currently be measured accurately. In some regions, lithology can be determined in relative terms (i.e., thick versus thin layers of an inferred type). Geologic mapping in Tyrrhena Terra has attempted to constrain the lithology of the terrain in which the valley networks are incised [*Mest and Crown*, 2006].

[50] Drainage densities (Tables 7a and 7b) for the 11 basins examined range from 0.004 km^{-1} (basin #74) to

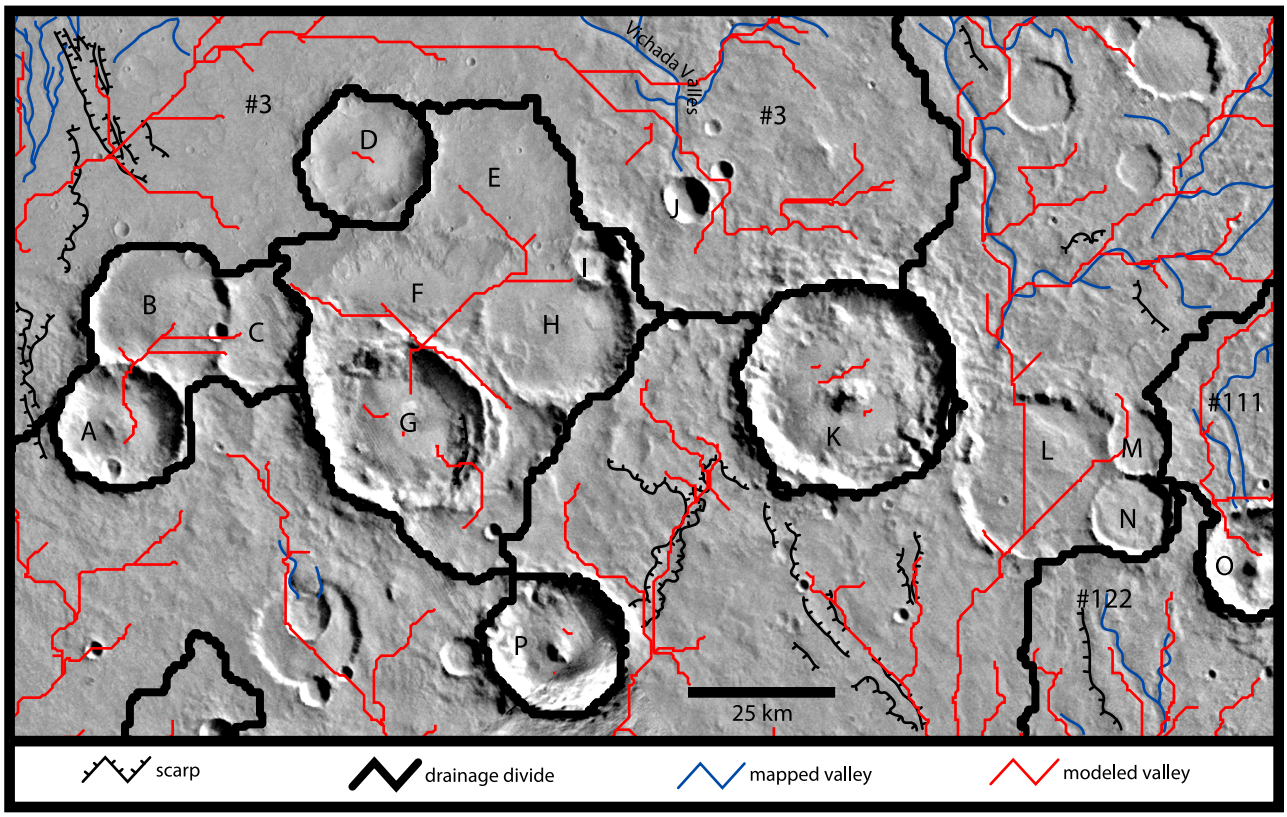

Figure 11. Map of geology (*Mest and Crown* [2006]), mapped and extracted (FAV = 2000) valleys, and delineated drainage divides (SFD = 575) covering part of Tyrrhena Terra study area. Here a cluster of 16 large craters (A-P) truncates Vichada Valles and other southerly flowing valleys. The algorithm shows a path for Vichada Valles to the west of the cluster, which is not observed in images. Using a SFD = 575 m, the sinks representing some craters (e.g., craters L and M) have been filled and valley pathways are delineated through them. Viking MDIM 2.0 photomosaic base; centered at 23.5°S, 272.8°W.

0.122 km^{-1} (basin #107) for mapped valleys (average = 0.043 km^{-1}), and 0.015 km^{-1} (basin #36) to 0.123 km^{-1} (basin #107) for extracted valleys (average = 0.046 km^{-1}). Here we use the DEM to delineate valleys within a watershed based purely on topography; thus, drainage densities calculated from extracted valley data can be considered to be the ideal densities for these basins, reflecting mature systems in idealized watersheds. This is effectively shown in Figure 12a as a function of drainage basin area. Furthermore, as mentioned previously, Figure 12a reinforces the idea that selection of a regional FAV is not typically an appropriate method to describe a group of individual watersheds. Stream lengths as a function of basin area (Figure 12b) show linear relationships for extracted streams but are more scattered for mapped streams. The consistency between extracted and mapped stream length ranges and maximum values for all of the basins examined help to characterize network-forming processes. These values indicate that trunk and tributary valleys are effectively "filling" basins by headward growth and suggest that in this part of the Martian highlands either one valley-forming process was dominant regionally, or multiple processes were actively eroding equally among the group of basins examined.

[51] Martian drainage densities were initially described qualitatively as "low" and decreasing toward higher latitudes [*Mars Channel Working Group*, 1983]. *Baker and Partridge* [1986] showed for sixteen small highland networks, densities ranged from 0.2 to 0.3 km^{-1}. *Cabrol and Grin* [2001] showed that 71 networks (including Vichada Valles) mapped at the 1:2M scale had similar drainage densities, ranging from 0.03 to 0.22 km^{-1}. However, according to *Carr* [1995, 1996], at the 1:2M scale, the most densely dissected areas of the Martian highlands yielded drainage densities of only 0.001 to 0.01 km^{-1}. *Carr and Chuang* [1997] mapped Martian networks at the 1:2M scale and drainage densities were found to be 0.0032 km^{-1} for Noachian units, 0.00047 km^{-1} for Hesperian units, and 0.00007 km^{-1} for Amazonian units. It should be noted that Carr and Chuang defined drainage density as the total valley length divided by the total area of a region of interest without outlining specific drainage basin areas. Only the most heavily dissected flanks of several Martian volcanoes had drainage densities (0.3 to 2.3 km^{-1}) similar to terrestrial values [*Gulick and Baker*, 1990]. Drainage densities derived in these previous studies are based on identification of valleys using Viking Orbiter images, whereas drainage densities determined in the following studies have incorporated high-resolution THEMIS and MOC images. *Grant* [2000] and *Grant and Parker* [2002] mapped valley networks in the Margaritifer Sinus region at larger scales than previous studies (1:500K) and consistently found low drainage densities, ranging from 0.03 to 0.11 km^{-1}. Drain-

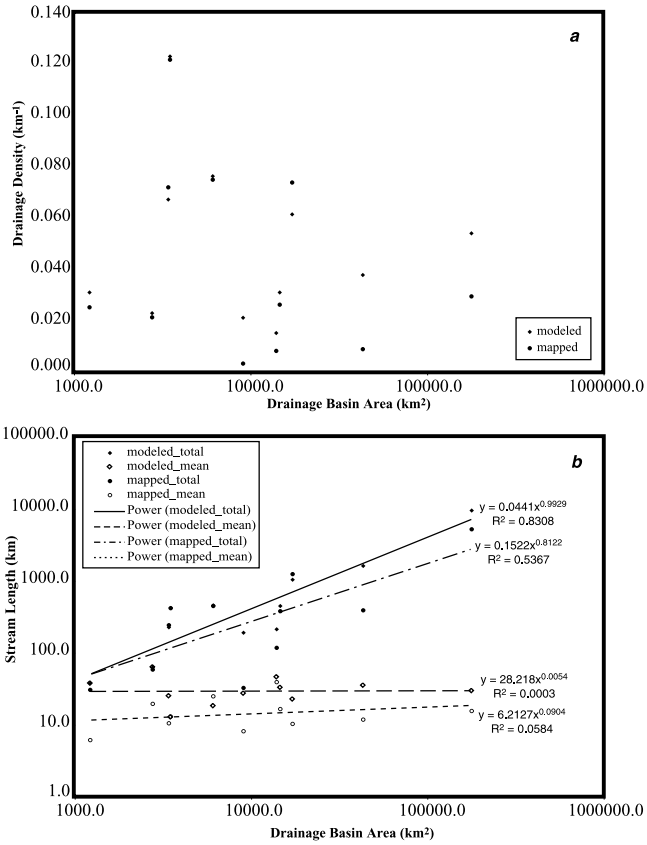

Figure 12. Plots of (a) drainage density and (b) stream length as a function of drainage basin area. For these data, model-predicted densities and stream lengths (total and average) tend to better approximate a straight line than mapped data, especially for drainage density. This is most likely due to the algorithm's inherent nature to delineate the most idealized networks based on the given DEM, and the values selected for the sink-fill depth and the accumulation threshold.

age densities ranging from 0.20 to 0.34 km^{-1} were determined for drainage basins in Terra Cimmeria [*Irwin and Howard*, 2002]; however, this range is for the "maximum" density based on defined areas and does not represent the total areas of representative drainage basins. Recent THEMIS day IR-based mapping of valley networks in the eastern Libya Montes [*Erkeling et al.*, 2009], Naktong Vallis and vicinity [*Yamaguchi et al.*, 2009], and Arabia Terra and Terra Meridiani [*Hoke and Hynek*, 2009] have found drainage densities of 0.123–0.232 km^{-1} (average = 0.148 km^{-1}) and 0.57 km^{-1} (5 well-preserved networks), 0.025–0.325 km^{-1}, and 0.053–0.14 km^{-1}, respectively.

[52] Recent studies calculating drainage densities from automatically extracted networks from MOLA topography were found to be 0.193 km^{-1} [*Craddock et al.*, 2001a, 2001b, 2003; average highlands, ±30° latitude], 0–0.12 km^{-1} [*Luo and Stepinski*, 2009; global), and 0.06 to 0.22 km^{-1} [*Stepinski and Collier*, 2003, 2004a, 2004b; twenty-six highland basins], comparable to densities calculated in the current and other studies of Martian drainage basins. Drainage densities calculated in this study and by the above mentioned authors are much lower than most terrestrial values (>2 km^{-1}) [*Schumm*, 1956; *Smith*, 1958; *Gregory and Walling*, 1973; *Morisawa*, 1962; *Gregory*, 1976; *Wohl*, 2000] but are comparable to values reported for some parts of the United States at 1:2M scale (0.149 km^{-1} for Arizona; 0.079 km^{-1} for Nebraska; 0.206 km^{-1} for New York; 0.119 km^{-1} for Texas; 0.209 km^{-1} for Washington) [*Carr and Chuang*, 1997], which include a wide range of climates (arid to temperate) and different geologic settings. *Stepinski et al.* [2002a, 2002b, 2003], *Collier et al.* [2003], and *Stepinski* [2003] compared the fractal nature of twenty Martian and nineteen terrestrial basins and found weak correlations between drainage density and dissipated potential energy but strong correlations between contributing area and stream length. Combined, these correlations suggest erosion and valley formation by rainfall was possible but was likely not sustained and uniformly distributed. Their results showed that either the observed surface reflects roughening by competing geologic processes (e.g., rainfall-driven erosion, impacts, eolian deposition) or that rainfall was minimally important and processes such as sapping or glacial/snowpack melt were the dominant erosional forces.

5.4. Stream Order and Bifurcation Ratio

[53] Stream orders were determined for mapped and extracted valleys using the Strahler ordering system [*Strahler*, 1964] and are defined by the following standard rules: fingertip tributaries are designated order 1, and the junction of two streams of the same order (u) forms a channel segment of the next higher order (u + 1). As defined by *Strahler* [1964], stream orders are useful because, in general, order number is directly proportional to the size of the contributing watershed, channel dimensions, and discharge anywhere within the network. Strahler stream orders for terrestrial system are generally low and range from 2 to 6 for mountain networks and 3 to 6 for lowland networks [*Wohl*, 2000]. The bifurcation ratio (R_b) is the ratio of the number of streams of a given order (N_u) to the number of streams of the next higher order (N_{u+1}) and can be used to estimate the number of streams of any given order and the total number of streams within a basin [*Horton*, 1945; *Strahler*, 1964; *Ritter et al.*, 1995]; the bifurcation ratio for an individual watershed (R_{bW}) is equal to the average of the bifurcation ratio values within the basin. In nature, bifurcation ratios range between 3.0 and 5.0 for watersheds in which the geology (lithology, structure, etc.) is relatively homogeneous and rarely is the theoretical minimum value of 2.0 approached under natural conditions. Geologic homogeneity within a basin would tend to form drainage systems that display morphometric and geometric similarities [*Strahler*, 1964].

[54] Mapped networks range from first to fourth order (Table 7a) and extracted networks range from first to fifth order (Table 7b). For nine basins, the numbers of streams (as a basin total) are higher for model-predicted watersheds, and two basins show higher numbers of streams for mapped watersheds. Stream orders and the log of the number of streams (summed for all 11 basins) plot as a straight line for both mapped and extracted streams (Figure 13a), which is typical of terrestrial drainage systems [e.g., *Schumm*, 1956; *Chorley*, 1957; *Morisawa*, 1962; *Strahler*, 1964]. The data show that the algorithm delineates more streams of all orders

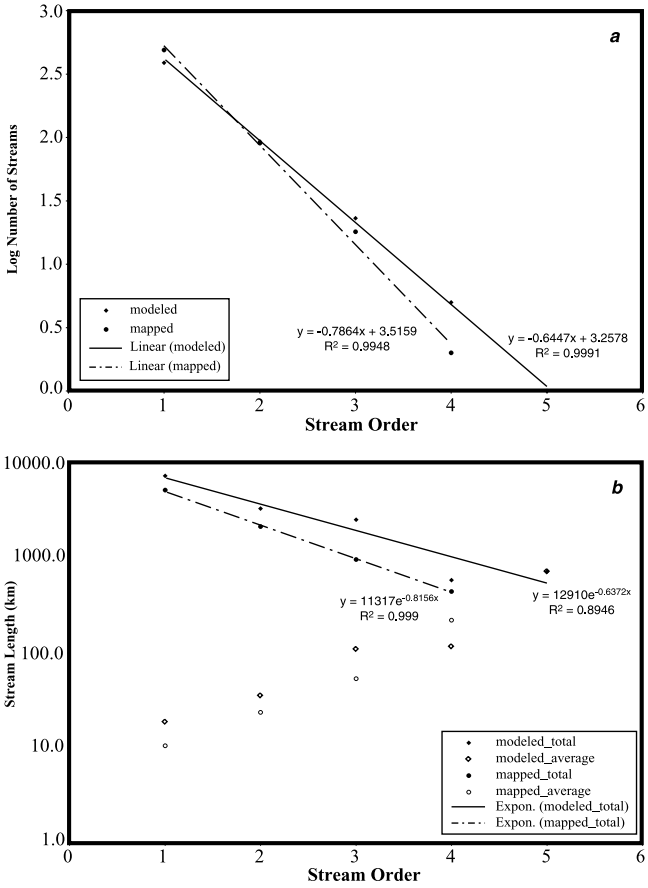

Figure 13. Plots of the (a) number of streams and (b) stream length as a function of stream order. The numbers of mapped streams show a slightly steeper slope than extracted streams in Figure 13a, but both data sets plot along straight lines. In Figure 13b, the lengths of mapped and extracted streams plot fairly close to straight lines and show typical inverse correlations for total (negative) and average (positive) stream lengths as a function of order. The relationships in Figures 13a and 13b are typical of terrestrial drainage systems [*Schumm*, 1956; *Chorley*, 1957; *Morisawa*, 1962; *Strahler*, 1964].

than are visible in images, producing higher-order networks (Table 7b).

[55] One difference between the mapped and extracted networks is that although the delineated drainage divides adequately enclose the mapped networks, there are several mapped valleys within the 11 basins that are not connected to the "main" systems within those basins. For example, basin #89 (Figures 10c and 10d) shows several first- and second-order mapped streams dissecting the crater that forms part of its divide as well as several streams that flow into and terminate along the rim of a buried impact crater. The algorithm does not identify all of these first- and second-order valleys and those that are identified are part of a single system. This partially accounts for overall lower orders for mapped networks and the differences in bifurcation ratios. Previous researchers found that Martian valley networks mapped at 1:2M and 1:500K scales using Viking Orbiter images were no greater than fourth-order [*Carr*, 1995, 1996; *Grant*, 2000; *Grant and Parker*, 2002].

[56] Several bifurcation ratios for extracted streams (Table 7b) in Tyrrhena Terra approach Strahler's theoretical minimum of 2.0 (range = 2.0–6.8), whereas only one mapped network (basin #130; Table 7a) approaches 2.0 (range = 2.0–6.7). This suggests that because the algorithm only accounts for topography, the algorithm misrepresents the effects of geology on valley formation by delineating features with "significant" topographic expressions (such as graben, the edges of or coalescing ejecta blankets, or closely spaced craters) as valleys. Thus, for this parameter, the mapped values provide a better evaluation of network formation than the extracted values since those misrepresentations can be eliminated by rigorous analysis of image data. Overall, from visual inspection of THEMIS daytime IR data, the surface geology (lithology and structure) for eight basins (#s 46, 51, 74, 89, 107, 111, 130, and 131) appears to be relatively homogeneous, where homogeneity is here expressed as a proportion of basin area covered by particular types of materials, such as plains or impact ejecta. Three basins (#s 3, 36, and 122) show some degree of heterogeneity at the surface by the presence of large amounts of ejecta deposits. In general, the relative bifurcation ratios for mapped networks (Table 7a) support this visual evaluation. For example, basin #3, identified with the largest contributing area in the study area, displays relatively homogeneous geology in THEMIS daytime IR images (mostly plains with various amounts of coverage by ejecta throughout the basin), whereas quantitatively, the bifurcation ratio for basin #3 (R_{bW} = 6.7) suggests the geology is slightly more hetereogeneous, which is supported by the presence of 30 craters (D > 10 km) that would have contributed to vertical and lateral mixing of near-surface materials and modification of the near-surface structure. This indicates that modeling alone cannot be used to characterize the hydrology of the Martian surface, but such characterizations require detailed geologic and geomorphic mapping to constrain the nature and relative ages of surface materials.

5.5. Relief Morphometry

[57] Relief characteristics, including relief ratio and ruggedness number, provide information about the overall steepness of a drainage basin and indicate the intensity of fluvial erosion operating on basin slopes [*Strahler*, 1964; *Ritter et al.*, 1995]. Measuring the relief of a drainage basin defines a slope value that provides an indication of runoff [*Ritter et al.*, 1995] and the potential energy of a drainage system [*Strahler*, 1964]. Maximum basin relief (H) is defined as the elevation difference between the highest point on the basin divide and the mouth of the trunk valley [*Strahler*, 1964]. The relief ratio (R_h) is the maximum basin relief (H) divided by the horizontal distance (L_b) along the longest dimension of the basin parallel to the principal drainage line [*Schumm*, 1956]. The ruggedness number (R) is the product of the maximum basin relief (H) and the drainage density (D_d) [*Melton*, 1957; *Strahler*, 1958, 1964].

[58] Maximum basin relief (Table 8) determined for the basins identified in this study ranges from 1,587 m for basin #130 to 4882 m for basin #122 (mean for 11 basins = 2656 km). Relief ratios for these basins (Table 8) range from 0.004 (basin #3) to 0.026 (basin #131) with an

Table 8. Relief Data for Extracted and Mapped Watersheds (SFD = 575)

Basin ID	FAV	L_b (km)	Maximum Basin Elevation (m)	Minimum Basin Elevation (m)	H (m)	R_h	R Extracted	R Mapped
131	2000	67	2116	355	1761	0.026	0.055	0.044
130	2000	100	358	−1230	1587	0.016	0.037	0.035
111	558	138	2345	−584	2929	0.021	0.196	0.211
107	190	108	2524	687	1837	0.017	0.226	0.224
46	400	156	2973	962	2012	0.013	0.153	0.151
74	5583	142	3351	1,461	1891	0.013	0.040	0.008
36	5583	129	3757	1,276	2481	0.019	0.037	0.022
51	2000	268	2371	252	2119	0.008	0.066	0.057
89[a]	775	274	3385	234	3151	0.012	0.195	0.233
122[a]	2000	379	3441	−1442	4882	0.013	0.186	0.044
3[a]	1000	1015	3745	−822	4567	0.004	0.247	0.137

[a]Most impact craters (D > 10 km) in these basins are postfluvial.

average = 0.015. For the 11 basins, ruggedness numbers range from 0.008 to 0.233 for mapped and 0.037 to 0.247 for extracted networks; average rugged numbers for mapped and extracted streams are 0.106 and 0.131, respectively. Other studies determined relief ratios (0.001–0.13) and ruggedness numbers (0.005–0.086) for drainage basins in Margaritifer Sinus [*Grant*, 2000; *Grant and Parker*, 2002] and were based on topography derived from Earth-based radar. Typical relief ratios for terrestrial basins range from 0.015 to 6.8 for mountain basins and 0.0004 to 0.01 for lowland basins; in general, $R_h \geq 0.02$ indicates mountain systems and $R_h \leq 0.02$ indicates lowland systems [*Wohl*, 2000]. Relief ratios calculated here are found to be comparable to those for Margaritifer Sinus [*Grant*, 2000; *Grant and Parker*, 2002] and comparable to terrestrial lowland networks and the low end of mountain systems [*Wohl*, 2000]. According to Table 2.3 in the study by *Wohl* [2000], terrestrial networks with R_h = 0.004–0.007 formed in humid temperate climates and in glacial sediments, or sedimentary or limestone bedrock, and networks R_h = 0.01–0.017 formed in semiarid climates or in clay shale substrate.

[59] Ruggedness numbers calculated in this study were higher for both mapped and model-predicted networks than determined for Margaritifer Sinus [*Grant*, 2000; *Grant and Parker*, 2002] and within the range (on the lower end) for terrestrial examples (0.03–10.9) [*Strahler*, 1964; *Grant*, 2000]. Low Martian ruggedness numbers (relative to terrestrial systems) have been attributed to low Martian drainage densities and imply that erosion by runoff may be inefficient due to surface and near-surface materials with high infiltration capacities and the ability to store large quantities of water [*Ritter et al.*, 1995; *Grant*, 2000]. In addition, *Strahler* [1958, 1964] noted that in order to obtain extremely high values of the ruggedness number, both maximum basin relief must be large (reflecting steep slopes) and drainage density must be high (reflecting large total stream length to basin area).

6. Conclusions

[60] We have completed geologic [*Mest and Crown*, 2006] and geomorphic mapping and hydrologic modeling of the highlands of Tyrrhena Terra, Mars. Valley and network morphology and morphometric parameters (drainage density, stream order, bifurcation ratio, and relief morphometry) have been determined for 11 drainage basins using both mapped and extracted data. These results, combined with geologic interpretations [*Mest and Crown*, 2006], have been used to constrain the processes that formed the valleys in this part of the highlands, as well as the climatic conditions in which they formed, and those conclusions are discussed here.

[61] The presence of valley networks, the establishment of integrated dendritic and (sub)parallel drainage patterns, and the distribution of valleys and eroded impact craters throughout Tyrrhena Terra suggests that fluvial dissection of the highlands was widespread and that significant amounts of fluids moved across the surface. Dendritic systems of valleys dissect low-gradient interlayered sedimentary, volcanic, and impact-related materials, and (sub)parallel networks are incised within steeper sloping materials, such as along the rims of impact craters. The observed Martian networks show that the accumulation of fluids into trunk streams was influenced primarily by topography. Based on mapping and image analysis, valleys in this region display degraded and pristine morphologies and a variety of crosscutting and superposition relations with impact craters. Morphologic observations, crater/valley relationships, impact crater distributions, and the lack of evidence for significant reactivation of valleys by later pulses of fluvial activity suggest that most Tyrrhena Terra valleys are ancient, most likely Noachian in age. Formation of gullies along the interior walls of many craters in the area, most of which head at or near-crater rims, unlike the gullies described by *Malin and Edgett* [2000], may represent younger fluvial activity, possibly extending into the Amazonian Period [*Mest and Crown*, 2005, 2006].

[62] Comparisons of mapped and model-predicted watersheds show that the Martian networks observed in images do not approach an idealized case of a precipitation-dominated system over large areas or of uniform, widespread dissection. As a first order attempt to identify watersheds on the present Martian surface, the hydrologic model used in this study appears to adequately delineate drainage divides and large-scale networks, at least down to second-order valleys. Delineation of drainage divides and valleys are affected by the spatial (64 pixels/degree) and vertical (~10 m) resolution of the MOLA DEM [*Smith et al.*, 2001]. As a result, the algorithm most accurately predicted valleys

greater than half a kilometer wide and 10 m deep. The hydrologic model shows widespread development of valley networks, which is inconsistent with large areas of apparently undissected terrain observed in images. Sink-fill depth and accumulation threshold selection are important factors in using the algorithm to best predict the locations, numbers, and patterns of mapped valleys; the sink-fill depth is a reflection of the scale at which watersheds are extracted. Application of this technique to other regions of Mars should involve automatic delineation of Martian watersheds on a basin-to-basin basis so as to maximize accuracy in valley delineation. Rigorous comparisons of the algorithm results to image data have helped to produce useful maps of Martian drainage basins and their associated valley networks. Additional valley segments may be identified using analyses of new (i.e., High Resolution Imaging Science Experiment (HiRISE), Context Camera (CTX), CRISM, and High Resolution Stereo Camera (HRSC)) data sets. It therefore seems necessary, given the combined inconsistencies and limitations of the topographic and image data sets that currently exist for Mars and Mars' complex geologic history, that hydrologic modeling of Martian terrains be accompanied by detailed geologic analyses and geomorphic mapping.

[63] Regardless of whether precipitation-driven runoff or groundwater sapping, or some combination of the two, formed valley networks in Tyrrhena Terra, it is clear that valley incision and maintenance of sustained flow were inefficient, potentially due to the following:

[64] • highly porous and (or) permeable surface materials coupled with local and regional variations in lithology as indicated by inter-basin and intrabasin variations in bifurcation and relief ratios, low ruggedness numbers, visual inspection of the near-surface geology, and the presence of pre-fluvial craters;

[65] • slopes that are low and therefore inadequate for efficient erosion and transport of debris;

[66] • competition between valley formation and other geologic processes, such as impact cratering, deposition of eolian sediments, and eolian and fluvial erosion, would have removed small valleys and subdue large valleys;

[67] • and temporal limitations controlled by climatic conditions that would have allowed only immature network development.

[68] Several lines of evidence support the inefficiency/lack of maturity of Martian watersheds in Tyrrhena Terra. Drainage densities (mapped: 0.004–0.122 km^{-1}; extracted: 0.015–0.123 km^{-1}) and Strahler stream orders (mapped: fourth order; extracted: fifth order) determined here, which are consistent with other studies of Martian valley networks, are much lower than for most terrestrial drainage basins. In addition, bifurcation ratios for most mapped networks show a similar range to typical terrestrial values (3.0–5.0). Combined with the geologic analysis of *Mest and Crown* [2006], these values suggest that valley networks in the Tyrrhena Terra study area are forming in geologically homogeneous basins, but the basin-to-basin differences in network morphology and morphometry indicate that the region is geologically heterogeneous.

[69] Low values for most of the parameters calculated in this study for mapped networks could be explained by smaller tributaries being removed by erosion [e.g., *Golombek et al.*, 2006] and/or deposition of dust (up to 3 m thick) [e.g., *Craddock and Maxwell*, 1993; *Jakosky et al.*, 2000; *Mellon et al.*, 2000], impact ejecta or midlatitude mantling-type deposits [e.g., *Mustard et al.*, 2001]. Dune-covered floors of Vichada Valles and crosscutting relationships with impact craters support deposition within this part of the highlands. Furthermore, the ability to identify the smallest fingertip valleys in images can be inhibited by image resolution and the spacecraft parameters (e.g., sun angle and incidence angle) at which images were acquired. Similarly, low ruggedness numbers, which are a function of drainage densities, suggest erosion by runoff was not very efficient in most basins due to low gradients or lithology and (or) that many of the smallest tributaries have been subsequently buried. However, even if most of the smallest tributaries (<1 m deep) were buried, a large number of intermediate-sized tributaries still remain unaccounted for and large areas of the intercrater plains remain undissected.

[70] The current investigation provides insight into processes of valley formation in the highlands of Tyrrhena Terra. Valleys in Tyrrhena Terra are found over a wide range of elevations suggesting fluid availability was not restricted to any specific elevation, as would be expected by sapping in which an aquifer typically intersects the surface over a limited elevation range. Many valleys head at or near the rims of craters, which argues against sapping because it is extremely difficult to establish a hydrologic head at the rim of a crater adequate enough to sustain sufficient flow to form valleys [e.g., *Craddock and Howard*, 2002]. Valley depths, widths, and morphologies vary along the lengths of most valleys, and some valleys appear to have eroded laterally in places, suggesting sustained flow. The overall low slopes and the likelihood that the lithology is relatively heterogeneous over much of the study area [*Mest and Crown*, 2006] suggest that surface materials have low resistance to erosion and (or) low surface permeability. This interpretation is supported by the basin-to-basin differences in the observed amount of dissection and resulting network patterns. In order for groundwater sapping to have been a significant component of valley formation in this part of the highlands, recharge of aquifers would have to have been very efficient. Discontinuous aquifers resulting from the interlayered nature of the local intercrater plains [*Mest and Crown*, 2006] or lack of an effective recharge mechanism would have limited sapping as a dominant valley-forming process. Furthermore, stream orders and relief ratios suggest that the basins in Tyrrhena Terra most closely resemble terrestrial lowland watersheds that dissect sediments or sedimentary rocks [*Wohl*, 2000], which are typically dominated by runoff processes, consistent with previous geologic interpretations of this terrain [*Mest and Crown*, 2006]. Rainfall on ancient Mars, as a process of valley network formation in Tyrrhena Terra, would require a thicker and warmer atmosphere and long-lived hydrologic cycle. Under cold and wet conditions, in which significant quantities of snow could generate runoff, a shallow permafrost layer would likely exist and effectively stagnate infiltration, thereby, discontinuing the supply of water for sapping, as suggested by *Irwin and Howard* [2002] in Terra Cimmeria, and increase runoff generated by snowmelt. It appears sapping may have only played a secondary role in valley formation in the highlands of Tyrrhena Terra. Therefore, precipitation-fed runoff, either directly by rainfall or by

snowmelt, is likely the dominant process of valley formation. Based on the spatial and temporal relationships of dissected highland materials and impact craters, erosion by runoff must have been widespread, but relatively short-lived with most activity within the Vichada Valles system confined to the Noachian Period.

[71] **Acknowledgments.** The authors would like to thank Herb Frey and the Planetary Geodynamics Laboratory for giving Scott Mest the opportunity to conduct research at Goddard Space Flight Center. Thoughtful and helpful reviews provided by Bob Craddock, Tomasz Stepinski, David Tarboton, and two anonymous reviewers considerably improved this manuscript. This research was supported by grants from the NASA Graduate Student Researchers Program (NGT5-125), the Planetary Geology and Geophysics Program (NAG5-10529), and the Pennsylvania Space Grant Consortium. MOC images courtesy of NASA/JPL/Malin Space Science Systems and THEMIS images courtesy of NASA/JPL/Arizona Sate University. MOLA data courtesy of NASA/GSFC.

References

Ansan, V., and N. Mangold (2004), Impact crater paleolakes in Hellas and Thaumasia Areas, Mars, 2nd Conf on Early Mars, Abstract 8006.

Ansan, V., N. Mangold, P. Masson, and G. Neukum, and the HRSC Team (2007), Topography of valley networks on Mars: Comparison between MOLA and HRSC DTM, Lunar and Planetary Science Conference, XXXVIII, Lunar and Planetary Institute, Houston, Abstract 1660 (CD-ROM).

Baker, V. R., and J. B. Partridge (1986), Small Martian valleys: Pristine and degraded morphology, *J. Geophys. Res.*, *91*, 3561–3572, doi:10.1029/JB091iB03p03561.

Banerdt, W. B., and A. Vidal (2001), Surface drainage on Mars, *Lunar and Planet. Sci. Conf.*, *XXXII*, Lunar and Planetary Institute, Houston, Tex, Abstract 1488(CD-ROM).

Bibring, J.-P., et al. (2006), Global mineralogical and aqueous Mars history derived from OMEGA/Mars Express data, *Science*, *312*, 400–404, doi:10.1126/science.1122659.

Boothroyd, J. C., and J. A. Grant (1985), Fluvial drainage basins and valley networks: Eastern Margaritifer Sinus, Reports of the Planetary Geology and Geophysics Program—1984, NASA Tech. Memo., *TM87563*, 316–318.

Brakenridge, G. R., H. E. Newsom, and V. R. Baker (1985), Ancient hot springs on Mars: Origins and paleoenvironmental significance of small Martian valleys, *Geology*, *12*, 859–862, doi:10.1130/0091-7613(1985)13<859:AHSOMO>2.0.CO;2.

Cabrol, N. A., and E. A. Grin (2001), Composition of the drainage network on early Mars, *Geomorphology*, *37*, 269–287, doi:10.1016/S0169-555X(00)00087-8.

Carr, M. H. (1995), The Martian drainage system and the origin of valley networks and fretted channels, *J. Geophys. Res.*, *100*, 7479–7507, doi:10.1029/95JE00260.

Carr, M. H. (1996), *Water on Mars*, 229 pp., Oxford Univ. Press, New York.

Carr, M. H., and F. C. Chuang (1997), Martian drainage densities, *J. Geophys. Res.*, *102*, 9145–9152, doi:10.1029/97JE00113.

Carr, M. H., and G. D. Clow (1981), Martian channels and valleys: Their characteristics, distribution, and age, *Icarus*, *48*, 91–117, doi:10.1016/0019-1035(81)90156-1.

Carr, M. H., and J. W. Head (2004), Formation of Martian valley networks: Melting of low to mid-latitude snowpacks during periods of high obliquity?, *Lunar and Planet. Sci. Conf.*, *XXXV*, Lunar and Planetary Institute, Houston, Tex, Abstract 1183(CD-ROM).

Carr, M. H., and M. C. Malin (2000), Meter-scale characteristics of Martian channels and valleys, *Icarus*, *146*, 366–386, doi:10.1006/icar.2000.6428.

Chorley, R. J. (1957), Climate and morphometry, *J. Geol.*, *65*, 628–638.

Clifford, S. M. (1993), A model for the hydrologic and climatic behavior of water on Mars, *J. Geophys. Res.*, *98*, 10,973–11,016, doi:10.1029/93JE00225.

Collier, M. L., T. F. Stepinski, S. M. Clifford, and P. J. McGovern (2003), Martian geomorphology from statistics of drainage networks, *Lunar and Planet. Sci. Conf.*, *XXXIV*, Lunar and Planetary Institute, Houston, Tex, Abstract 1642(CD-ROM).

Costard, F., F. Poulet, J.-P. Bibring, D. Baratoux, N. Mangold, S. Meresse, P. Pinet, and the Omega team (2006), Detection of hydrated minerals on fluidized ejecta lobes from Omega observations: Implications in the history of Mars, *Lunar and Planet. Sci. Conf.*, *XXXVII*, Lunar and Planetary Institute, Houston, Abstract 1288(CD-ROM).

Craddock, R. A., and A. D. Howard (2002), The case for rainfall on a warm, wet early Mars, *J. Geophys. Res.*, *107*(E11), 5111, doi:10.1029/2001JE001505.

Craddock, R. A., and T. A. Maxwell (1993), Geomorphic evolution of the Martian highlands through ancient fluvial processes, *J. Geophys. Res.*, *98*, 3453–3468, doi:10.1029/92JE02508.

Craddock, R. A., T. A. Maxwell, and A. D. Howard (1997a), The early history of Mars as told by degraded highland impact craters, in *Conference on Early Mars: Geologic and Hydrologic Evolution, Physical and Chemical Environments, and the Implications for Life*, LPI Contrib. No. 916, 20–21.

Craddock, R. A., T. A. Maxwell, and A. D. Howard (1997b), Crater morphometry and modification in the Sinus Sabaeus and Margaritifer Sinus region of Mars, *J. Geophys. Res.*, *102*, 13,321–13,340, doi:10.1029/97JE01084.

Craddock, R. A., T. A. Maxwell, and A. D. Howard (1999), The evidence for climatic variations on early Mars, *Lunar and Planet. Sci. Conf.*, *XXX*, Lunar and Planetary Institute, Houston, Tex, Abstract 1977(CD-ROM).

Craddock, R. A., G. A. Franz, A. C. Cook, and A. D. Howard (2001a), High resolution morphometric studies of Martian valley networks in the Iapygia region, *Lunar and Planet. Sci. Conf.*, *XXXII*, Lunar and Planetary Institute, Houston, Abstract 1833(CD-ROM).

Craddock, R. A., R. P. Irwin, and A. D. Howard (2001b), Martian drainage densities: Analyses from MOLA digital elevation models, Workshop on the Martian Highlands and Mojave Desert Analogs, October 20–27, 2001, Las Vegas, NV and Barstow, CA, Abstract 4016.

Craddock, R. A., R. P. Irwin, and A. D. Howard (2003), Characteristics of Martian valley networks and the implications for past climates, *Lunar and Planet. Sci. Conf.*, *XXXIV*, Lunar and Planetary Institute, Houston, Abstract 1888(CD-ROM).

Crown, D. A., L. F. Bleamaster III, and S. C. Mest (2005), Styles and timing of volatile-driven activity in the eastern Hellas region of Mars, *J. Geophys. Res.*, *110*, E12S22, doi:10.1029/2005JE002496.

Crown, D. A., L. F. Bleamaster III, S. C. Mest, and J. F. Mustard (2009) Geologic mapping of the NW rim of Hellas Basin, Mars, *Lunar and Planet. Sci. Conf.*, *XL*, Lunar and Planetary Institute, Houston, Tex, Abstract 1705(CD-ROM).

De Hon, R. A. (2002), Martian sedimentary basins and regional watersheds, *Lunar and Planet. Sci. Conf.*, *XXXIII*, Lunar and Planetary Institute, Houston, Tex, Abstract 1915(CD-ROM).

Erkeling, G., D. Reiss, H. Hiesinger, and R. Jaumann (2009), Morphologic, stratigraphic and morphometric investigations in eastern Libya Montes, Mars: Implications for long-term fluvial activity, *Lunar and Planet. Sci. Conf.*, *XL*, Lunar and Planetary Institute, Houston, Tex, Abstract 1604(CD-ROM).

Erskine, R. H., T. R. Green, J. A. Ramirez, and L. H. MacDonald (2006), Comparison of grid-based algorithms for computing upslope contributing area, *Water Resour. Res.*, *42*, W09416, doi:10.1029/2005WR004648.

Fairfield, J., and P. Leymarie (1991), Drainage networks from grid digital elevation models, *Water Resour. Res.*, *27*, 709–717, doi:10.1029/90WR02658.

Fassett, C. I., and J. W. Head (2007), Valley formation on Martian volcanoes in the Hesperian: Evidence for melting of summit snowpack, caldera lake formation, drainage and erosion on Ceraunius Tholus, *Icarus*, *189*, 118–135, doi:10.1016/j.icarus.2006.12.021.

Fassett, C. I., and J. W. Head (2008), Valley network-fed, open-basin lakes on Mars: Distribution and implications for Noachian surface and subsurface hydrology, *Icarus*, *198*, 37–56, doi:10.1016/j.icarus.2008.06.016.

Forsythe, R. D., and C. R. Blackwelder (1998), Closed drainage crater basins of the Martian highlands: Constraints on the early Martian hydrologic cycle, *J. Geophys. Res.*, *103*, 31,421–31,431, doi:10.1029/98JE01966.

Frey, H., L. Hutchison, S. Sakimoto, and J. Roark (2000), A large population of possible buried impact basins on Mars revealed by MOLA topographic data, *Lunar and Planet. Sci. Conf.*, *XXXI*, Lunar and Planetary Institute, Houston, Tex, Abstract 1736(CD-ROM).

Goldspiel, J. M., and S. W. Squyres (2000), Groundwater sapping and valley formation on Mars, *Icarus*, *148*, 176–192, doi:10.1006/icar.2000.6465.

Goldspiel, J. M., S. W. Squyres, and D. G. Jankowski (1993), Topography of small Martian valleys, *Icarus*, *105*, 479–500, doi:10.1006/icar.1993.1143.

Golombek, M. P., et al. (2006), Erosion rates at the Mars Exploration Rover landing sites and long-term climate change on Mars, *J. Geophys. Res.*, *111*, E12S10, doi:10.1029/2006JE002754.

Grant, J. A. (2000), Valley formation in Margaritifer Sinus, Mars, by precipitation-recharged ground-water sapping, *Geology*, *28*, 223–226, doi:10.1130/0091-7613(2000)28<223:VFIMSM>2.0.CO;2.

Grant, J. A., and T. J. Parker (2002), Drainage evolution in the Margaritifer Sinus region, Mars, *J. Geophys. Res.*, *107*(E9), 5066, doi:10.1029/2001JE001678.

Grant, J. A., and P. H. Schultz (1990), Gradational epochs on Mars: Evidence from west-northwest of Isidis Basin and Electris, *Icarus*, *84*, 166–195, doi:10.1016/0019-1035(90)90164-5.

Grant, J. A., and P. H. Schultz (1993), Degradation of selected terrestrial and Martian impact craters, *J. Geophys. Res.*, *98*, 11,025–11,042, doi:10.1029/93JE00121.

Greeley, R., and J. E. Guest (1987), Geologic map of the eastern equatorial region of Mars, U.S. Geol. Surv. Misc. Inv. Ser. Map I-1802B, scale 1:15M.

Gregory, K. J. (1976), Drainage networks and climate, in *Geomorphology and Climate*, edited by E. Derbyshire, pp. 289–315, Wiley-Interscience, Chinchester.

Gregory, K. J., and D. E. Walling (1973), *Drainage Basin Form and Process*, 456 pp., Halsted Press, New York.

Gulick, V. C. (1998), Magmatic intrusions and a hydrothermal origin for fluvial valleys on Mars, *J. Geophys. Res.*, *103*, 19,365–19,387, doi:10.1029/98JE01321.

Gulick, V. C. (2001), Origin of the valley networks on Mars: A hydrological perspective, *Geomorphology*, *37*, 241–268, doi:10.1016/S0169-555X(00)00086-6.

Gulick, V. C., and V. R. Baker (1990), Origin and evolution of valleys on Martian volcanoes, *J. Geophys. Res.*, *95*, 14,325–14,344, doi:10.1029/JB095iB09p14325.

Gulick, V. C., D. Tyler, C. P. McKay, and R. M. Haberle (1997), Episodic ocean-induced CO2 pulses on Mars: Implications for fluvial valley formation, *Icarus*, *130*, 68–86, doi:10.1006/icar.1997.5802.

Gyasi-Agyei, Y., G. Willgoose, and F. P. de Troch (1995), Effects of vertical resolution and map scale of digital elevation models on geomorphological parameters used in hydrology, *Hydrol. Process.*, *9*, 363–382.

Hartmann, W. K. (1971), Martian cratering III: Theory of crater obliteration, *Icarus*, *15*, 410–428, doi:10.1016/0019-1035(71)90119-9.

Hoke, M. R. T. and B. M. Hynek (2009), Analyzing and dating valley networks in Arabia Terra and Terra Meridiani, Mars, *Lunar and Planet. Sci. Conf.*, *XXXIX*, Lunar and Planetary Institute, Houston, Abstract 2183 (CD-ROM).

Horton, R. E. (1932), Drainage basin characteristics, *Trans. Am. Geophys. Union*, *13*, 350–361.

Horton, R. E. (1945), Erosional development of streams and their drainage basins: Hydrophysical approach to quantitative morphology, *Geol. Soc. Am. Bull.*, *56*, 275–370, doi:10.1130/0016-7606(1945)56[275:EDOSAT]2.0.CO;2.

Hynek, B. M., and R. J. Phillips (2001), Evidence for extensive denudation of the Martian highlands, *Geology*, *29*, 407–410, doi:10.1130/0091-7613(2001)029<0407:EFEDOT>2.0.CO;2.

Irwin, R. P., and R. A. Craddock (2001), Drainage basin integration in the Martian highlands, Workshop on the Martian Highlands and Mojave Desert Analogs, 20–27 October 2001, Las Vegas, Nev, and Barstow, Calif, Abstract 4013.

Irwin, R. P., and A. D. Howard (2002), Drainage basin evolution in Noachian Terra Cimmeria, Mars, *J. Geophys. Res.*, *107*(E7), 5056, doi:10.1029/2001JE001818.

Irwin, R. P., and T. A. Maxwell (2003), Multiple generations of Martian valley networks: Reconciling extensive fluvial erosion with immature drainage systems, Sixth International Conference on Mars, Lunar and Planetary Institute, Houston, Tex, Abstract 3243.

Irwin, R. P., A. D. Howard, T. A. Maxwell, and R. A. Craddock (2002a), Drainage basin disruption and re-integration processes in the Martian highlands, *Lunar and Planet. Sci. Conf.*, *XXXIII*, Lunar and Planetary Institute, Houston, Tex, Abstract 1729(CD-ROM).

Irwin, R. P., T. A. Maxwell, A. D. Howard, R. A. Craddock, and D. W. Leverington (2002b), A large paleolake basin at the head of Ma'adim Vallis, Mars, *Science*, *296*, 2209–2212, doi:10.1126/science.1071143.

Irwin, R. P., A. D. Howard, and T. A. Maxwell (2004), Geomorphology and hydraulics of Ma'adim Vallis, Mars, during a Noachian/Hesperian boundary paleoflood, *Lunar and Planet. Sci. Conf.*, *XXXV*, Lunar and Planetary Institute, Houston, Tex, Abstract 1852(CD-ROM).

Jakosky, B. M., M. T. Mellon, H. H. Kieffer, P. R. Christensen, E. S. Varnes, and S. W. Lee (2000), The thermal inertia of Mars from the Mars Global Surveyor Thermal Emission Spectrometer, *J. Geophys. Res.*, *105*, 9643–9652, doi:10.1029/1999JE001088.

Jenson, S. K. (1991), Applications of hydrologic information automatically extracted from digital elevation models, *Hydrol. Process.*, *5*, 31–44, doi:10.1002/hyp.3360050104.

Jenson, S. K., and J. O. Domingue (1988), Extracting topographic structure from digital elevation data for Geographic Information System analysis, *Photogramm. Eng. Remote Sens.*, *54*, 1593–1600.

Kelson, K. I., and S. G. Wells (1989), Geologic influence on fluvial hydrology and bedload transport in small mountain watersheds, northern New Mexico, *Earth Surf. Process. Landf.*, *14*, 671–690, doi:10.1002/esp.3290140803.

Kenward, T., D. P. Lettenmaier, E. F. Wood, and E. Fielding (2000), Effects of digital elevation model accuracy on hydrologic predictions, *Remote Sens. Environ.*, *74*, 432–444, doi:10.1016/S0034-4257(00)00136-X.

Kochel, R. C., and J. F. Piper (1986), Morphology of large valleys on Hawaii: Evidence for groundwater sapping and comparisons with Martian valleys, *J. Geophys. Res.*, *91*, E175–E192, doi:10.1029/JB091iB13p0E175.

Kochel, R. C., A. D. Howard, and C. McLane (1985), Channel networks developed by groundwater sapping in fine-grained sediments: Analogs to some Martian valleys, in *Models in Geomorphology*, edited by M. J. Woldenberg, pp. 313–341, Allen and Unwin, Boston.

Leonard, G. J., and K. L. Tanaka (2001), Geologic map of the Hellas region of Mars, U.S. Geol. Surv. Geol. Inv. Ser. Map I-2694, scale 1:5M.

Luo, W., and T. F. Stepinski (2009), Global, computer-generated map of valley networks on Mars, *Lunar and Planet. Sci. Conf.*, *XL*, Lunar and Planetary Institute, Houston, Tex, Abstract 1311(CD-ROM).

Malin, M. C., and M. H. Carr (1999), Groundwater formation of Martian valleys, *Nature*, *397*, 589–591, doi:10.1038/17551.

Malin, M. C., and K. S. Edgett (2000), Evidence for recent groundwater seepage and surface runoff on Mars, *Science*, *288*, 2330–2335, doi:10.1126/science.288.5475.2330.

Mark, D. M. (1988), Network Models in Geomorphology, in *Modeling in Geomorphological Systems*, John Wiley.

Mars Channel Working Group (1983), Channels and valleys on Mars, *Geol. Soc. Am. Bull.*, *94*, 1035–1054, doi:10.1130/0016-7606(1983)94<1035:CAVOM>2.0.CO;2.

Martz, L. W., and J. Garbrecht (1998), The treatment of flat areas and depressions in automated drainage analysis of raster digital elevation models, *Hydrol. Process.*, *12*, 843–855, doi:10.1002/(SICI)1099-1085(199805)12:6<843::AID-HYP658>3.0.CO;2-R.

Masursky, H. (1973), An overview of geological results from Mariner 9, *J. Geophys. Res.*, *78*, 4009–4030, doi:10.1029/JB078i020p04009.

Maxwell, T. A., and R. A. Craddock (1995), Age relations of Martian highland drainage basins, *J. Geophys. Res.*, *100*, 11,765–11,780, doi:10.1029/95JE00940.

McCauley, J. F., M. H. Carr, J. A. Cutts, W. K. Hartmann, H. Masursky, D. J. Milton, R. P. Sharp, and D. E. Wilhelms (1972), Preliminary Mariner 9 report on the geology of Mars, *Icarus*, *17*, 289–327, doi:10.1016/0019-1035(72)90003-6.

Mellon, M. T., B. M. Jakosky, H. H. Kieffer, and P. R. Christensen (2000), High-resolution thermal inertia mapping from the Mars Global Surveyor Thermal Emission Spectrometer, *Icarus*, *148*, 437–455, doi:10.1006/icar.2000.6503.

Melton, M. A. (1957), An analysis of the relations among elements of climate, surface properties, and geomorphology, *Project NR 389–042, Tech. Rept. 11*, 100 pp., Columbia Univ., Dept. of Geology, ONR, Geography Branch, New York.

Mest, S. C. (2004), Evolution of the Martian highlands: Implications from drainage basin characteristics and valley network morphologies, Ph.D. Dissertation, 294 pp., Univ. of Pittsburgh, Pittsburgh, Pa.

Mest, S. C., and D. A. Crown (2001a), Fluvial degradation of the circum-Hellas highlands of Mars, Workshop on the Martian Highlands and Mojave Desert Analogs, 20–27 October 2001, Las Vegas, Nev, and Barstow, Calif, Abstract 4014.

Mest, S. C., and D. A. Crown (2001b), Geology of the Reull Vallis region, Mars, *Icarus*, *153*, 89–110, doi:10.1006/icar.2001.6655.

Mest, S. C., and D. A. Crown (2005), Millochau crater, Mars: Infilling and erosion of an ancient highland impact crater, *Icarus*, *175*, 335–359, doi:10.1016/j.icarus.2004.12.008.

Mest, S. C., and D. A. Crown (2006), Geologic Map of MTM-20272 and -25272 Quadrangles, Terra Tyrrhena Region of Mars, U.S. Geol. Surv. Sci. Inv. Map I-2934, scale 1:1,004,000.

Mest, S. C., D. A. Crown, and W. Harbert (2001a), Highland drainage basins and valley networks in the eastern Hellas region of Mars, *Lunar and Planet. Sci. Conf.*, *XXXII*, Lunar and Planetary Institute, Houston, Tex, Abstract 1457(CD-ROM).

Mest, S. C., W. Harbert, and D. A. Crown (2001b), Application of Geographical Information System Arc/Info grid-based surface hydrologic modeling to the eastern Hellas region, Mars, *EOS Trans. AGU*, *82*, Spring Meet. Suppl., Abstract P31A–05.

Mest, S. C., D. A. Crown, and W. Harbert (2002), Fluvial degradation of the highlands: The Terra Tyrrhena region of Mars, *Lunar and Planet. Sci. Conf.*, *XXXIII*, Lunar and Planetary Institute, Houston, Tex, Abstract 1892(CD-ROM).

Mest, S. C., D. A. Crown, L. F. Bleamaster, and J. F. Mustard (2008), Morphology, morphometry, and distribution of craters in NW Hellas, Mars, *Lunar and Planet. Sci. Conf.*, *XXXIX*, Lunar and Planetary Institute, Houston, Tex, Abstract 1704(CD-ROM).

Milton, D. J. (1973), Water and processes of degradation in the Martian landscape, *J. Geophys. Res.*, *78*, 4037–4047, doi:10.1029/JB078i020p04037.

Molloy, B. I., and T. F. Stepinski (2007), Automated mapping of valley networks on Mars, *Comput. Geosci.*, *33*, 728–738, doi:10.1016/j.cageo.2006.09.009.

Moore, J. M., and A. D. Howard (2005), Large alluvial fans on Mars, *J. Geophys. Res.*, *110*, E04005, doi:10.1029/2004JE002352.

Moore, J. M., and D. E. Wilhelms (2001), Hellas as a possible site of ancient ice-covered lakes on Mars, *Icarus*, *154*, 258–276, doi:10.1006/icar.2001.6736.

Morisawa, M. E. (1962), Quantitative geomorphology of some watersheds in the Appalachian Plateau, *Geol. Soc. Am. Bull.*, *73*, 1025–1046, doi:10.1130/0016-7606(1962)73[1025:QGOSWI]2.0.CO;2.

Mustard, J. F., C. D. Cooper, and M. K. Rifkin (2001), Evidence for recent climate change on Mars from the identification of youthful near-surface ground ice, *Nature*, *412*, 411–413, doi:10.1038/35086515.

O'Callaghan, J. F., and D. M. Mark (1984), The extraction of drainage networks from digital elevation data, *Comput. Vis. Graph. Image Process.*, *28*, 323–344, doi:10.1016/S0734-189X(84)80011-0.

Pelkey, S. M., et al. (2007), CRISM observations of hydrated crater deposits in Terra Tyrrhena, Mars, *Lunar and Planet. Sci. Conf.*, *XXXVIII*, Lunar and Planetary Institute, Houston, Abstract 1994(CD-ROM).

Pieri, D. C. (1976), Martian channels: Distribution of small channels in the Martian surface, *Icarus*, *27*, 25–50, doi:10.1016/0019-1035(76)90182-2.

Pieri, D. C. (1980), Martian valleys: Morphology, distribution, age, and origin, *Science*, *210*, 895–897, doi:10.1126/science.210.4472.895.

Ritter, D. F., R. C. Kochel, and J. R. Miller (1995), *Process Geomorphology*, 540 pp., Wm. C. Brown Publishers, Dubuque, IA.

Schaber, G. G. (1977), Geologic map of the Iapygia Quadrangle, Mars, U.S. Geol. Surv. Misc. Inv. Ser. Map I-1020, scale 1:5M.

Schumm, S. A. (1956), The evolution of drainage systems and slopes in badlands at Perth Amboy, New Jersey, *Geol. Soc. of Amer. Bull.*, *67*, 597–646.

Smith, D. E., et al. (1999), The global topography of Mars and implications for surface evolution, *Science*, *284*, 1495–1503, doi:10.1126/science.284.5419.1495.

Smith, D. E., et al. (2001), Mars Orbiter Laser Altimeter: Experiment summary after the first year of global mapping of Mars, *J. Geophys. Res.*, *106*, 23,689–23,722, doi:10.1029/2000JE001364.

Smith, K. G. (1958), Erosional processes and landforms in Badlands National Monument, South Dakota, *Geol. Soc. Am. Bull.*, *69*, 975–1008, doi:10.1130/0016-7606(1958)69[975:EPALIB]2.0.CO;2.

Snyder, J. P. (1982), *Map projections used by the U.S. Geological Survey*, 313 pp., Geol. Surv. Bull. 1532.

Soille, P., J. Vogt, and R. Colombo (2003), Carving and adaptive drainage enforcement of grid digital elevation models, *Water Resour. Res.*, *39*(12), 1366, doi:10.1029/2002WR001879.

Stepinski, T. F. (2003), Vertical analysis of Martian drainage basins, *Lunar and Planet. Sci. Conf.*, *XXXIV*, Lunar and Planetary Institute, Houston, Abstract 1659(CD-ROM).

Stepinski, T. F., and M. L. Collier (2003), Drainage densities of computationally extracted Martian drainage basins, Sixth International Conference on Mars, Lunar and Planetary Institute, Houston, Abstract 3100 (CD-ROM).

Stepinski, T. F., and M. L. Collier (2004a), Extraction of Martian valley networks from digital topography, *J. Geophys. Res.*, *109*, E11005, doi:10.1029/2004JE002269.

Stepinski, T. F., and M. L. Collier (2004b), Computational analysis of drainage basins on Mars: Appraising the drainage density, *Lunar and Planet. Sci. Conf.*, *XXXV*, Lunar and Planetary Institute, Houston, Abstract 1168(CD-ROM).

Stepinski, T. F., and S. Coradetti (2004), Systematic differences in topography of Martian and terrestrial drainage basins, *Lunar and Planet. Sci. Conf.*, *XXXV*, Lunar and Planetary Institute, Houston, Tex, Abstract 1166(CD-ROM).

Stepinski, T. F., M. M. Marinova, P. J. McGovern, and S. M. Clifford (2002a), The fractal characteristics of Martian drainage basins: Implications for the timing, intensity, and duration of rainfall, *Lunar and Planet. Sci. Conf.*, *XXXIII*, Lunar and Planetary Institute, Houston, Tex, Abstract 1347(CD-ROM).

Stepinski, T. F., M. M. Marinova, P. J. McGovern, and S. M. Clifford (2002b), Fractal analysis of drainage basins on Mars, *Geophys. Res. Lett.*, *29*(8), 1189, doi:10.1029/2002GL014666.

Stepinski, T. F., R. Vilalta, M. Achari, and P. J. McGovern (2003), Algorithmic classification of drainage networks on Mars and its relation to Martian geological units, *Lunar and Planet. Sci. Conf.*, *XXXIV*, Lunar and Planetary Institute, Houston, Tex, Abstract 1653(CD-ROM).

Strahler, A. N. (1952), Hypsometric (area-altitude) analysis of erosional topography, *Geol. Soc. Am. Bull.*, *63*, 1117–1142, doi:10.1130/0016-7606(1952)63[1117:HAAOET]2.0.CO;2.

Strahler, A. N. (1954), Quantitative geomorphology of erosional landscapes, 19th. Internat. Geol. Cong. (Algiers), Compte Rendus, Fascicule XV, 341–354.

Strahler, A. N. (1957), Quantitative analysis of watershed geomorphology, *Am. Geophys. Union Trans.*, *38*, 913–920.

Strahler, A. N. (1958), Dimensional analysis applied to fluvially eroded landforms, *Geol. Soc. Am. Bull.*, *69*, 279–300, doi:10.1130/0016-7606(1958)69[279:DAATFE]2.0.CO;2.

Strahler, A. N. (1964), Part II. Quantitative geomorphology of drainage basins and channel networks, in *Handbook of Applied Hydrology: A Compendium of Water-resource Technology*, edited by V. T. Chow, pp. 39–76, McGraw-Hill.

Tanaka, K. L., and G. J. Leonard (1995), Geology and landscape evolution of the Hellas region of Mars, *J. Geophys. Res.*, *100*, 5407–5432, doi:10.1029/94JE02804.

Tanaka, K. L., J. M. Dohm, J. H. Lias, and T. M. Hare (1998), Erosional valleys in the Thaumasia region of Mars: Hydrothermal and seismic origin, *J. Geophys. Res.*, *103*, 31,407–31,420, doi:10.1029/98JE01599.

Tarboton, D. G., R. L. Bras, and I. Rodriguez-Iturbe (1991), On the extraction of channel networks from digital elevation data, *Hydrol. Process.*, *5*, 81–100, doi:10.1002/hyp.3360050107.

Thieken, A. H., A. Lücke, B. Diekkrüger, and O. Richter (1999), Scaling input data by GIS for hydrological modeling, *Hydrol. Process.*, *13*, 611–630, doi:10.1002/(SICI)1099-1085(199903)13:4<611::AID-HYP758>3.0.CO;2-6.

Tucker, G. E., and R. L. Bras (1998), Hillslope processes, drainage density, and landscape morphology, *Water Resour. Res.*, *34*, 2571–2564, doi:10.1029/98WR01474.

Turcotte, R., J.-P. Fortin, A. N. Rousseau, S. Massicotte, and J.-P. Villeneuve (2001), Determination of the drainage structure of a watershed using a digital elevation model and a digital river and lake network, *J. Hydrol. Amsterdam*, *240*, 225–242, doi:10.1016/S0022-1694(00)00342-5.

Vogt, J. V., R. Colombo, and F. Bertolo (2003), Deriving drainage networks and catchment boundaries: A new methodology combining digital elevation data and environmental characteristics, *Geomorphology*, *53*(3–4), 281–298, doi:10.1016/S0169-555X(02)00319-7.

Wang, X., and Z. Yin (1998), A comparison of drainage networks derived from digital elevation models at two scales, *J. Hydrol. Amsterdam*, *210*, 221–241, doi:10.1016/S0022-1694(98)00189-9.

Wilson, S. A., A. D. Howard, J. M. Moore, and J. A. Grant (2007), Geomorphic and stratigraphic analysis of Crater Terby and layered deposits north of Hellas basin, Mars, *J. Geophys. Res.*, *112*, E08009, doi:10.1029/2006JE002830.

Wohl, E. (2000), *Mountain Rivers*, 320 pp., AGU, Washington, D.C.

Yamaguchi, Y., H. Miyamoto, K. L. Tanaka, and J. A. Palmero Rodriguez (2009), Mapping valley networks in the Noachian terrain around Naktong Vallis, Mars: Topographic control on drainage density, *Lunar and Planet. Sci. Conf.*, *XL*, Lunar and Planetary Institute, Houston, Abstract 1630(CD-ROM).

D. A. Crown and S. C. Mest, Planetary Science Institute, 1700 E. Ft. Lowell Rd., Ste. 106, Tucson, AZ 85719-2395, USA. (mest@psi.edu)

W. Harbert, Department of Geology and Planetary Science, University of Pittsburgh, 200 SRCC Bldg., 4107 O'Hara St., Pittsburgh, PA 15260-3332, USA.